

Structure and Infrastructure Engineering

Maintenance, Management, Life-Cycle Design and Performance

ISSN: (Print) (Online) Journal homepage: <https://www.tandfonline.com/loi/nsie20>

Impact of asymmetrical corrosion of piers on seismic fragility of ageing irregular concrete bridges

Ebrahim Afsar Dizaj, Mohammad R. Salami & Mohammad M. Kashani

To cite this article: Ebrahim Afsar Dizaj, Mohammad R. Salami & Mohammad M. Kashani (29 Oct 2023): Impact of asymmetrical corrosion of piers on seismic fragility of ageing irregular concrete bridges, Structure and Infrastructure Engineering, DOI: [10.1080/15732479.2023.2271887](https://doi.org/10.1080/15732479.2023.2271887)

To link to this article: <https://doi.org/10.1080/15732479.2023.2271887>



© 2023 The Author(s). Published by Informa UK Limited, trading as Taylor & Francis Group



Published online: 29 Oct 2023.



Submit your article to this journal [↗](#)



Article views: 336






View related articles [↗](#)



View Crossmark data [↗](#)

Impact of asymmetrical corrosion of piers on seismic fragility of ageing irregular concrete bridges

Ebrahim Afsar Dizaj^{a,b} , Mohammad R. Salami^c  and Mohammad M. Kashani^b 

^aDepartment of Civil Engineering, Azarbaijan Shahid Madani University, Tabriz, Iran; ^bFaculty of Engineering and Physical Sciences, University of Southampton, Southampton, United Kingdom; ^cSchool of Engineering and the Built Environment, Birmingham City University, Birmingham, United Kingdom

ABSTRACT

This article investigates the seismic fragility of ageing irregular multi-span reinforced concrete (RC) bridges. Different irregularity sources are considered, including: (i) substructure stiffness irregularity arising from the unequal-height piers, (ii) substructure stiffness irregularity arising from the spatially variable (asymmetrical) corrosion damage of piers and (iii) irregular distribution of effective tributary masses on piers of varying heights. To this end, a three-dimensional nonlinear finite element model is developed for multi-span RC bridges and verified against a large-scale shake table test results of a two-span concrete bridge specimen available in the literature. Nonlinear pushover, incremental dynamic and seismic fragility analyses are performed on three groups of two-span RC bridges with different configurations. Moreover, a time-dependent dimensionless local damage index is employed to evaluate the failure sequence and collapse probability of selected bridge layouts. The analysis results of the three studied irregularity sources show the considerable significance of spatially variable corrosion of bridge piers and substructure irregularity on the failure sequence of piers and seismic fragility of multi-span RC bridges. Furthermore, analysis outcomes show that uneven corrosion of piers triggers an unbalanced distribution of seismic ductility demands and irregular seismic response of equal-height multi-span RC bridges.

ARTICLE HISTORY

Received 25 March 2023
Revised 31 May 2023
Accepted 27 June 2023

KEYWORDS

Fragility analysis;
irregularity; local damage
index; multi-span bridge;
nonlinear dynamic;
reinforced concrete;
spatially variable corrosion





1. Introduction

One of the main challenges in bridge industry is the design of bridges located in seismic regions and varying topography terrains such as mountainous areas or steep-sided overcrossings. Based on the current construction practice, the specific design solution is to build such bridges with irregular substructures, i.e. unequal height piers (Kappos, Manolis, & Moschonas, 2002). However, the asymmetric height distribution in such bridges triggers unbalanced seismic ductility demands across the dissimilar height piers. Consequently, the non-uniform superstructure movement due to the higher lateral load attraction of stiffer piers results in a complex dynamic response of irregular RC bridges (Akbari, 2010; Guirguis & Mehanny, 2013).

Current design philosophy in existing design codes such as AASHTO (2012), California Department of Transportation, (2013) and Eurocode 8 (CEN 1998-2, 2005) provides specific provisions to control bridge seismic irregularities. These provisions aim to prevent damage accumulation in stiffer members and ensure the near-synchronised collapse of piers at a given target seismic demand. For instance, AASHTO (2012) limits the ratio between the

effective stiffness of adjacent bridge piers within bent or adjacent bents within a bridge frame. Some consequences of disregarding code requirements are described by Xiang and Li (2020). However, there are circumstances in which structural engineers need to design and evaluate bridge structures with specific geometrical characteristics (e.g., relative stiffness of piers) beyond the seismic design code recommendations. For such cases, linear analysis methods are not applicable, and more sophisticated nonlinear analysis methods are needed to accurately evaluate the seismic behaviour of irregular bridge structures.

Several studies are available in the literature on the seismic performance of irregular RC bridges (Hu & Guo, 2020; Sajed & Tehrani, 2020; Soltanieh, Memarpour, & Kilanehi, 2019). The findings of previous studies confirm the higher vulnerability of irregular bridges compared to regular bridges (Akbari, 2012). Afsar Dizaj, Salami, and Kashani (2022a) investigated the influence of bridge layout on the seismic vulnerability of irregular multi-span RC bridges. The outcome of this study showed that the failure probability of bents significantly depends on the height arrangement of piers. Akbari and Maalek (2018) reviewed state-of-the-art proposed irregularity indices for irregular RC bridges.

CONTACT Ebrahim Afsar Dizaj  ebrahim.afsardizaj@azaruniv.ac.ir  Azarbaijan Shahid Madani University, Tabriz, Iran;  ebrahim.afsardizaj@soton.ac.uk  University of Southampton, University Road, Highfield Campus, Southampton, UK.

© 2023 The Author(s). Published by Informa UK Limited, trading as Taylor & Francis Group

This is an Open Access article distributed under the terms of the Creative Commons Attribution-NonCommercial-NoDerivatives License (<http://creativecommons.org/licenses/by-nc-nd/4.0/>), which permits non-commercial re-use, distribution, and reproduction in any medium, provided the original work is properly cited, and is not altered, transformed, or built upon in any way. The terms on which this article has been published allow the posting of the Accepted Manuscript in a repository by the author(s) or with their consent.

Moreover, different methodologies have been proposed in the literature to balance the irregular seismic response of RC bridges with unequal height piers (Guirguis & Mehanny, 2013; Ishac & Mehanny, 2017; Jara, Villanueva, Jara, & Olmos, 2013; Priestley, 2007; Mitoulis & Rodriguez, 2017; Xiang & Li, 2020).

Furthermore, environmental stressors such as aggressive conditions in the marine environment or using de-icing salt on the road in winter negatively impact the integrity of transport infrastructure. This is more significant in structures such as concrete bridges in moderate to high seismic regions (ASCE, 2021; Ghosh & Sood, 2016). The corrosion-induced damage in highway concrete bridges imposes a considerable annual maintenance and rehabilitation cost worldwide (Schmitt, 2009). Additionally, it has been known as the leading cause of catastrophic failure of some RC bridges (Domaneschi et al., 2020). The outcome of static cyclic loading tests (Liu, Jiang, & He, 2017; Meda, Mostosi, Rinaldi, & Riva, 2014) and shaking table experiments conducted on corrosion-damaged RC columns (Ge, Dietz, Alexander, & Kashani, 2020) have indicated a significant reduction in the strength and ductility of test specimens. Moreover, many studies have concluded the higher failure probability of corroded RC structures (Afsar Dizaj & Kashani, 2022a; Dizaj, Padgett, & Kashani, 2021; Cui, Zhang, Ghosn, & Xu, 2018; Zhang, Akiyama, Shintani, Xin, & Frangopol, 2021).

Depending on the location and exposure conditions, a multi-span RC bridge might be exposed to spatially variable corrosion of piers over its service life. This phenomenon is more likely to occur in bridges of unequal height piers in steep-sided river valleys, where different piers might be directly or indirectly exposed to chloride ions attack. For example, some piers might be in a river, and others are in a road or valley. Given the stiffness degradation of corrosion-damaged RC components, such spatially variable corrosion of piers might expose the bridge to an uneven accumulation of damage and asynchronous failure. Therefore, depending on the time-dependent corrosion damage in different piers of a multi-span concrete bridge, the spatially variable corrosion of piers can worsen/mitigate the seismic irregularity of such bridges. Moreover, the spatially variable corrosion of bridge substructure might trigger an irregular seismic response of a multi-span RC bridge with a regular pristine configuration. However, such aspects have not been investigated in previous studies, and the symmetrical corrosion scenario of bridge piers has been assumed in nonlinear analyses (Choe, Gardoni, Rosowsky, & Haukaas, 2009; Zhang, DesRoches, & Tien, 2019). The main reason for such shortcomings in the previous studies was the lack of advanced finite element models with suitable nonlinear material models to capture corrosion damage accurately.

The above discussion shows a significant scarcity in the literature to investigate the seismic fragility of irregular multi-span RC bridges subject to spatially variable corrosion of piers. Furthermore, the possible consequences of spatially variable corrosion of bridge piers on the regular seismic response of equal-height pier multi-span RC bridges have not been investigated. To address these shortcomings, this

article investigates the effect of three different sources of bridge seismic irregularity, such as (i) substructure stiffness irregularity, (ii) spatially variable corrosion of bridge piers and (iii) unequal distribution of super-imposed masses across different bridge bents. Additionally, a time-dependent local dimensionless damage index is employed to study the spatially variable corrosion effects on the seismic fragility of bents of varying heights.

Towards this goal, in Section 2, an advanced three-dimensional nonlinear finite element model for multi-span irregular RC bridges is developed and validated by large-scale shake table test results of a two-span unequal height RC bridge specimen (Johnson, Ranf, Saiidi, Sanders, & Eberhard, 2008). Then, in Section 3, different irregular bridge configurations combined with different spatially variable corrosion scenarios are considered. Subsequently, the validated model is used for nonlinear pushover analysis (in Section 4) and incremental dynamic and seismic fragility analysis (in Section 5) on different considered bridge layouts. Finally, the influence of considered irregularities on the seismic fragility of RC bridges is investigated. Analyses results show that spatially variable corrosion of piers significantly affects the nonlinear dynamic response, seismic performance and vulnerability of both regular and irregular multi-span RC bridges.

2. Finite element model and verification

2.1. Details of the benchmark RC bridge shake table experimental test

In this study, the geometrical layout of an experimentally tested two-span RC bridge is considered a benchmark for seismic performance evaluation of multi-span RC bridges with irregular substructures. Figure 1 presents the 3D views of the multi-span RC bridge and the considered bridge specimen. This bridge system was tested under multiple transverse excitation loading using the shake table facility at the University of Nevada, Reno (Johnson et al., 2008). As Figure 1 shows, the bridge structure consists of three bents with variable pier heights, where the stiffer bent (with shorter piers) is placed on the right side, the medium-height bent on the left side and the tallest bent at the middle of the bridge. The superstructure is composed of three parallel deck beams in each span. Moreover, some super-imposed masses were placed on the superstructure to induce an axial load ratio ($N_u/(A_g \sigma_c)$) of 0.082 in all the piers; where N_u is the applied compressive axial load on each pier, A_g is the gross cross-sectional area of each pier and σ_c is the compressive strength of concrete.

Figure 2 depicts the geometrical details of each bent and pier. As shown in Figure 2, all the piers have the same cross-sectional details, where the diameter of each pier is 305 mm, the ratio of longitudinal reinforcements is 1.56% and the volumetric ratio of spirals is 0.9%. Each bent was placed on a separate shake table for running the experimental test. In total, 20 successive tests were conducted on the bridge, where the intensity of input excitation was incrementally increased in each test. Except for a test conducted bidirectionally, in the remaining 19 tests, the input

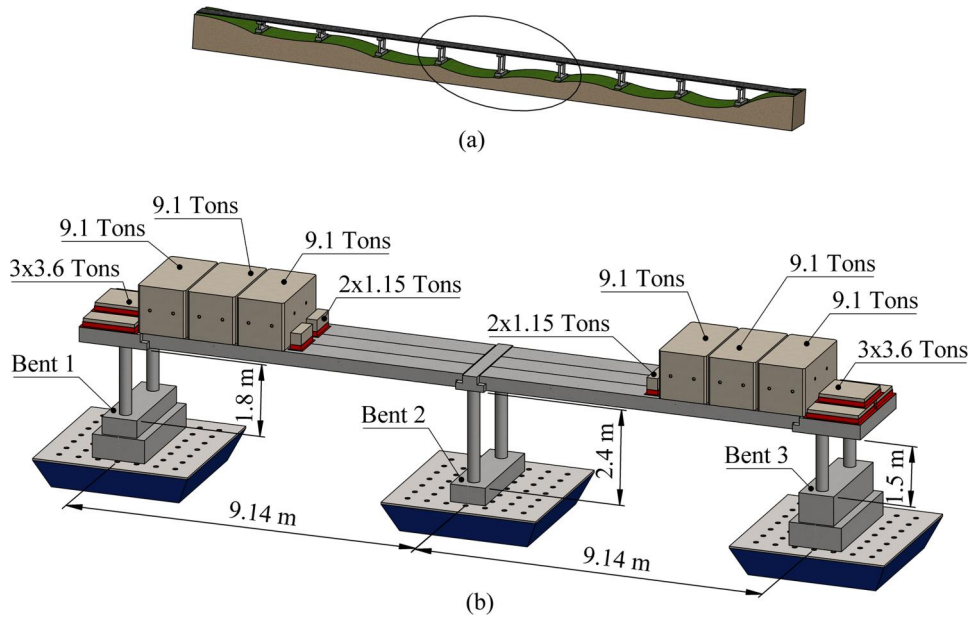


Figure 1. Three-dimensional views of prototype location in a multi-span bridge (a) and the two-span RC bridge specimen tested by Johnson et al. (2008) (b).

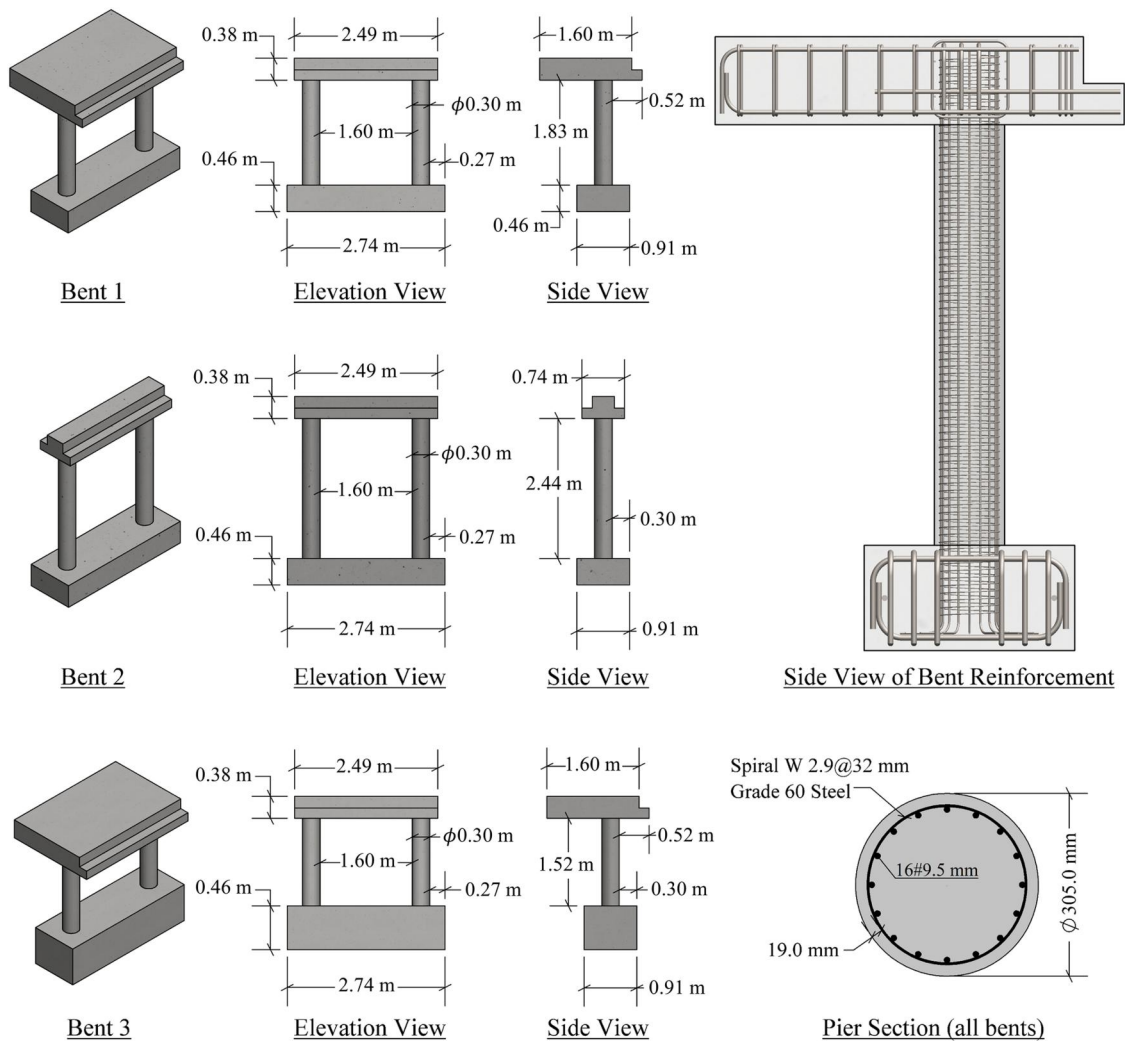


Figure 2. Geometrical details of bents and piers of the two-span RC bridge tested by Johnson et al. (2008).

acceleration history was applied in the transverse direction (West-East direction). Detailed information on the experimental setup and details of the bridge specimen is available in Johnson et al. (2008).

2.2. Proposed finite element model

The details and configuration of the bridge specimen tested by Johnson et al. (2008) are adopted as a benchmark to simulate the nonlinear response of multi-span RC bridges with irregular substructures. Typically, the superstructure (deck beams and beam caps) is designed to remain in the elastic range in each bridge system. However, piers are the most critical elements in a bridge that determine the nonlinear seismic response of the system. Therefore, special attention should be paid to the accurate modelling of piers in the nonlinear modelling of a bridge system. Towards this matter, the nonlinear fibre beam-column element proposed by Kashani, Lowes, Crewe, and Alexander (2016) is adopted here to simulate the nonlinear behaviour of bridge piers. This model can simulate the degradation in cyclic behaviour of RC columns due to inelastic buckling and low-cycle fatigue of longitudinal reinforcements. The accuracy of this model has been verified against an extensive number of experimental cyclic test results on uncorroded and corroded RC column specimens (Dizaj, Madandoust, & Kashani, 2018b, Afsar Dizaj & Kashani, 2022b).

Figure 3 displays the proposed nonlinear finite element model of bridge piers established in OpenSees (McKenna, 2011). Figure 3 shows that each pier model consists of five force-based elements and a rigid link. The zero-length section elements are used in the top and bottom of the pier to simulate the bar-slip behaviour of longitudinal reinforcement in connection regions. Two force-based elements, each with a length of $6L_{eff}$ and three integration points (IPs), are

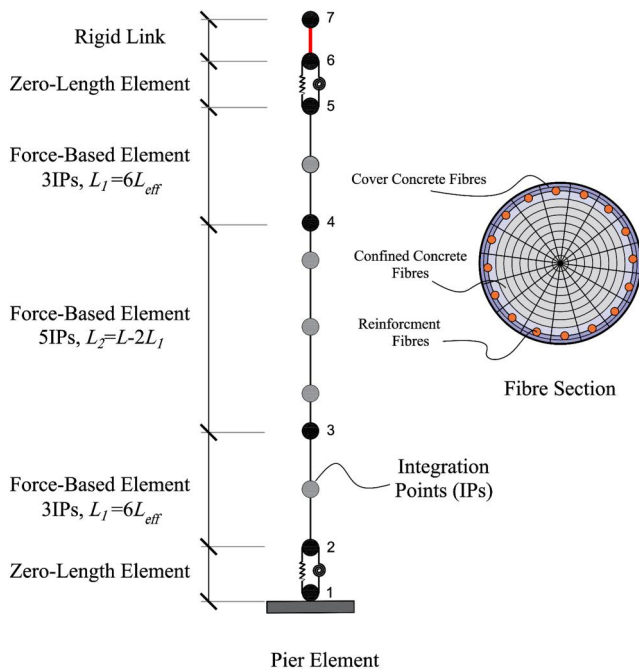


Figure 3. Fibre discretisation model of bridge piers.

used in the critical top and bottom zones. L_{eff} is the effective buckling length of the longitudinal reinforcements determined using the algorithm proposed by Dhakal and Maekawa, (2002). The middle element is also a force-based element with 5 IPs. On top of the pier, a rigid link is used to model the rigid connection (between the pier and beam cap) zone. At each integration point, the cross-section of the pier is divided into several patches (fibres), including unconfined cover concrete patches, confined concrete patches and reinforcement patches.

The nonlinear stress-strain behaviour of cover and core concrete is modelled using the uniaxial model *Concrete04*, available in OpenSees. This model considers a linear stiffness degradation for unloading/reloading and exponential decay for the tensile strength based on the model proposed by Karsan and Jirsa (1969). Moreover, the compressive stress-strain model of concrete is defined using Popovic's proposed envelope. The compressive strength and spalling strain of unconfined concrete are assumed to be 40.8 MPa and 0.004, respectively. Moreover, the mechanical properties of concrete are modified using the model proposed by Mander, Priestley, and Park (1988) to account for the confinement effect.

The nonlinear stress-strain behaviour of steel rebars is simulated using the buckling model developed by Kashani, Lowes, Crewe, and Alexander (2015). This model can simulate the post-buckling softening behaviour of longitudinal reinforcement in compression and the low-cycle fatigue degradation of steel rebars. Further details about the material model of reinforcing bars can be found in Kashani et al. (2015). Figure 4 presents the three-dimensional finite element model of the benchmark RC bridge specimen. All the piers are modelled using the fibre beam-column model shown in Figure 3. The superstructure components are modelled using the elastic beam-column elements, where the gross cross-sectional area and moment of inertia of deck and cap beams are used to define the geometrical characteristics of these components. Furthermore, several rigid links (10 links in total) perpendicular to the longitudinal direction of deck beam elements are defined to assign the superimposed weights in their accurate centre of mass. The pier-to-cap beam connection and the pier-to-foundation connection regions are assumed to be fully fixed.

2.3. Implementation of time-dependent corrosion damage in the bridge model

In order to take into account the adverse influence of corrosion on the performance of RC bridges, the structural details of bridge piers should be updated based on the level of corrosion. The corrosion level is generally described in terms of the mass loss ratio of reinforcement, which can be obtained from:

$$\psi(t_p) = 1 - \frac{A_{ave}(t_p)}{A_0} \quad (1)$$

where $\psi(t_p)$ is the time-dependent mass loss ratio of reinforcement; t_p (in years) is the time from corrosion

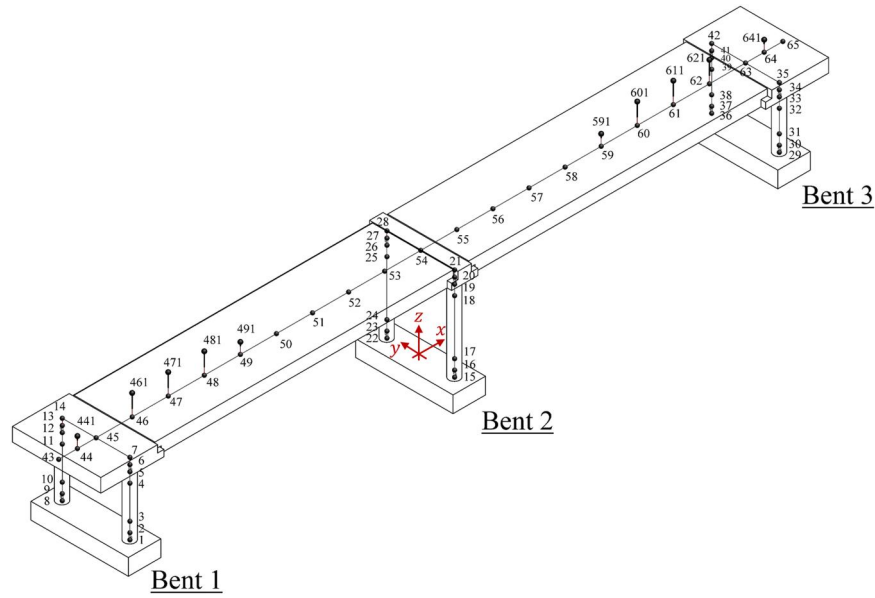


Figure 4. Three-dimensional finite element model of benchmark RC bridge.

initiation of longitudinal rebars, and A_0 and $A_{ave}(t_p)$ are an initial and average time-dependent cross-sectional area of steel reinforcement, respectively. Employing the empirical relationship proposed by Vu and Stewart (2000) for time-dependent corrosion current density, $A_{ave}(t_p)$ can be calculated using (Afsar Dizaj, 2022):

$$A_{ave}(t_p) = \left(\frac{D_L X - 1.05(1 - W/C)^{-1.64} t_p^{0.71}}{D_L X} \right)^2 A_0 \quad (2)$$

where D_L is the diameter of uncorroded longitudinal bars; X is the thickness of cover concrete and W/C is the water-cement ratio.

The pitting corrosion effects can be included by applying a pitting coefficient β as follows:

$$A(t_p) = \beta A_{ave}(t_p) \quad (3)$$

where $A(t_p)$ is the time-dependent cross-sectional area of reinforcement, including pitting corrosion effects. According to outcomes of a 3D optical scanning technique conducted by Kashani, Crewe, and Alexander (2013) on 23 corroded bars, the pitting coefficient (β) follows a lognormal distribution with median (μ_β) and standard deviation (σ_β) as:

$$\mu_\beta = \exp \left(a [\psi(t_p)]^{1.83} + 0.5b^2 [\psi(t_p)]^{2.34} \right) \quad (4)$$

$$\sigma_\beta = \left[\exp \left(c [\psi(t_p)]^{1.83} + b^2 [\psi(t_p)]^{2.34} \right) \right] \left[\exp \left(b^2 [\psi(t_p)]^{2.34} - 1 \right) \right] \quad (5)$$

where a , b and c are regression coefficients with values of -0.00052 , 0.00065 and -0.00104 (Kashani et al., 2013). By having $\psi(t_p)$ for each time in the service life of a bridge, the mechanical properties of cover and core concrete, the mechanical properties of reinforcements (both in tension and compression), and the diameter ($D_L(t_p)$) and cross-sectional area of reinforcement can be modified for each time since corrosion initiation (t_p). With the updated mechanical and geometrical properties of the material, the effective buckling

Table 1. Material properties of different components.

Component	σ_c (MPa)	σ_y (MPa)	σ_u (MPa)	σ_{yh} (MPa)	E_c (MPa)
Pier	40.8	459	669	462	30185
Cap Beam	48.2	–	–	–	32888
Deck Beam	49.8	–	–	–	32888

length of reinforcement can be calculated using the procedure provided by Dhakal and Maekawa (2002). Therefore effective slenderness ratio ($L_{eff}/D_L(t_p)$) and the fatigue life characteristics of corroded longitudinal rebars can be calculated. Further details are available in the systematic modeling guidelines provided by Afsar Dizaj and Kashani (2022b).

In the current study, the mean value of structural details is considered to calculate $\psi(t_p)$, and the mean value of β is used in Eq. (3) to modify the cross-sectional area of corroded reinforcing bars. Previous study by Dizaj, Madandoust, and Kashani (2018a) indicated that the uncertainties associated with spatial variability of pitting corrosion and randomness associated with structural uncertainties have negligible impact on the seismic fragility of corroded structures compared with the influence of uncertainties associated with input ground motions. Moreover, this article is a comparative scenario-based study focusing mainly on the impact of spatially variable corrosion of bridge piers on the seismic fragility of multi-span bridges. Therefore, using the mean value of probabilistic parameters is suitable, where the effects of pitting corrosion are modelled by modifying the mechanical properties of steel and concrete.

2.4. Validation of the proposed three-dimensional bridge model

To examine the accuracy of the developed finite element model of the benchmark bridge, the material properties and geometrical dimensions are assigned to each component based on the information provided by Johnson et al. (2008).

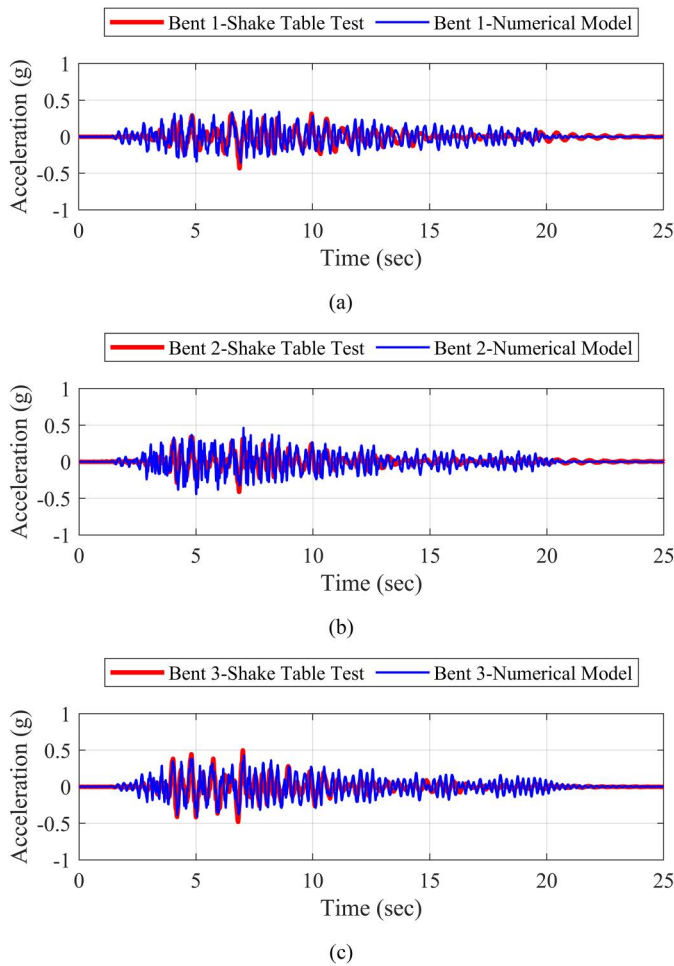


Figure 5. Validation of the numerical model against the shake table test results: (a) bent 1; (b) bent 2 and (c) bent 3.

The properties of the materials used in the analyses are provided in Table 1, i.e. the compressive strength of concrete (σ_c), the yield strength of longitudinal reinforcements (σ_y), the ultimate tensile strength of longitudinal reinforcements (σ_u), the yield strength of spiral reinforcements (σ_{yh}) and the modulus of elasticity of concrete (E_c). Using the developed model, the acceleration response of the superstructure during shake table tests is simulated and compared with those measured in the experiment.

Figure 5 illustrates the comparison of the numerical model with experimental test data. In this figure, as an example, the simulated acceleration response of superstructure at the top of bent 1, bent 2 and bent 3 in test 17 is compared with the corresponding response measured in the shake table test. As shown in Figure 5, the numerical simulation results show a very good match in terms of the value and timing of the peak acceleration responses to the experimental results. This confirms the validity of the proposed numerical modelling methodology in the accurate prediction of the nonlinear seismic response of the benchmark bridge. In the next section, employing the developed finite element model, different layouts of the benchmark bridge are considered to investigate the influence of spatially variable corrosion of piers on the seismic performance and fragility of irregular bridge systems.

3. Scenario-based case study bridges

Different structural layouts are considered here to investigate the influence of spatially variable corrosion of piers on the transverse seismic response of RC bridges with irregular mass and stiffness. The first layout is a bridge with stiffness irregularity and unequal mass distribution across the superstructure length. The label of this bridge is IS-UM (Irregular Stiffness & Unequal Mass distribution). A schematic 2D view of this bridge is shown in Figure 6a. The IS-UM bridge has the same details as the benchmark bridge (as shown in Figures 1 and 2). The only difference between the IS-UM bridge and the benchmark bridge is the placement of the piers, where the tallest piers are placed in bent 1, the shortest piers are placed in bent 3, and the medium-height piers are placed in bent 2.

The aim of considering different layouts compared to the benchmark bridge is to investigate the influence of another arrangement of unequal height piers on failure sequence and seismic response of multi-span RC bridges. To consider the influence of spatially variable corrosion of piers, three cases with different corrosion levels are considered for IS-UM bridge such as: (i) case 1: where the bridge is uncorroded in its pristine condition, (ii) case 2: where the piers in bent 1 and 2 are slightly corroded while the piers of bent 3 are severely corroded and (iii) case 3: where the piers in bent 1 and bent 3 are slightly corroded while the piers in bent 2 are severely corroded.

It should be noted that the attributed corrosion levels (pristine, slight corrosion and severe corrosion) are a representative description of the observed extent of damage in the experimentally tested corroded RC components (Afsar Dizaj, Salami, & Kashani, 2022b). For example, the 20% corroded RC piers tested by Meda et al. (2014) show more than 50% ductility reduction. Therefore, the mass loss percentage of about 20% is considered an extreme corrosion condition. Categorising corrosion levels below 20% into three groups, the mass loss percentages below $\sim 7\%$ can be classified as slight corrosion, the mass loss percentages between 7% and $\sim 15\%$ as moderate corrosion and higher levels of corrosion as severe corrosion. Adopting this classification, using Eq. (1), the mass loss ratios corresponding to $t_p=5$ years (which translates to $\psi=5.5\%$) and $t_p=30$ years (which translates to $\psi=19\%$) are considered as slight and severe corrosion conditions for bridge piers, respectively. The W/C is assumed to be 0.4 in mass loss ratio calculations.

The second considered bridge type, RS-UM (Regular Stiffness & Unequal Mass distribution), is a regular bridge with uniform-height piers and unequal distribution of superstructure masses. The geometry of the RS-UM bridge is shown in Figure 6b. The height of all piers is assumed to be equal to that of the medium-height piers in the benchmark bridge. The reason for considering this layout is to study the significance of spatially variable corrosion of piers on the seismic performance of regular RC bridges. Two cases (case 4 and case 5) are considered toward this target. In case 4, the RS-UM bridge is in its pristine condition. In case 5, the RS-UM is subjected to spatially variable

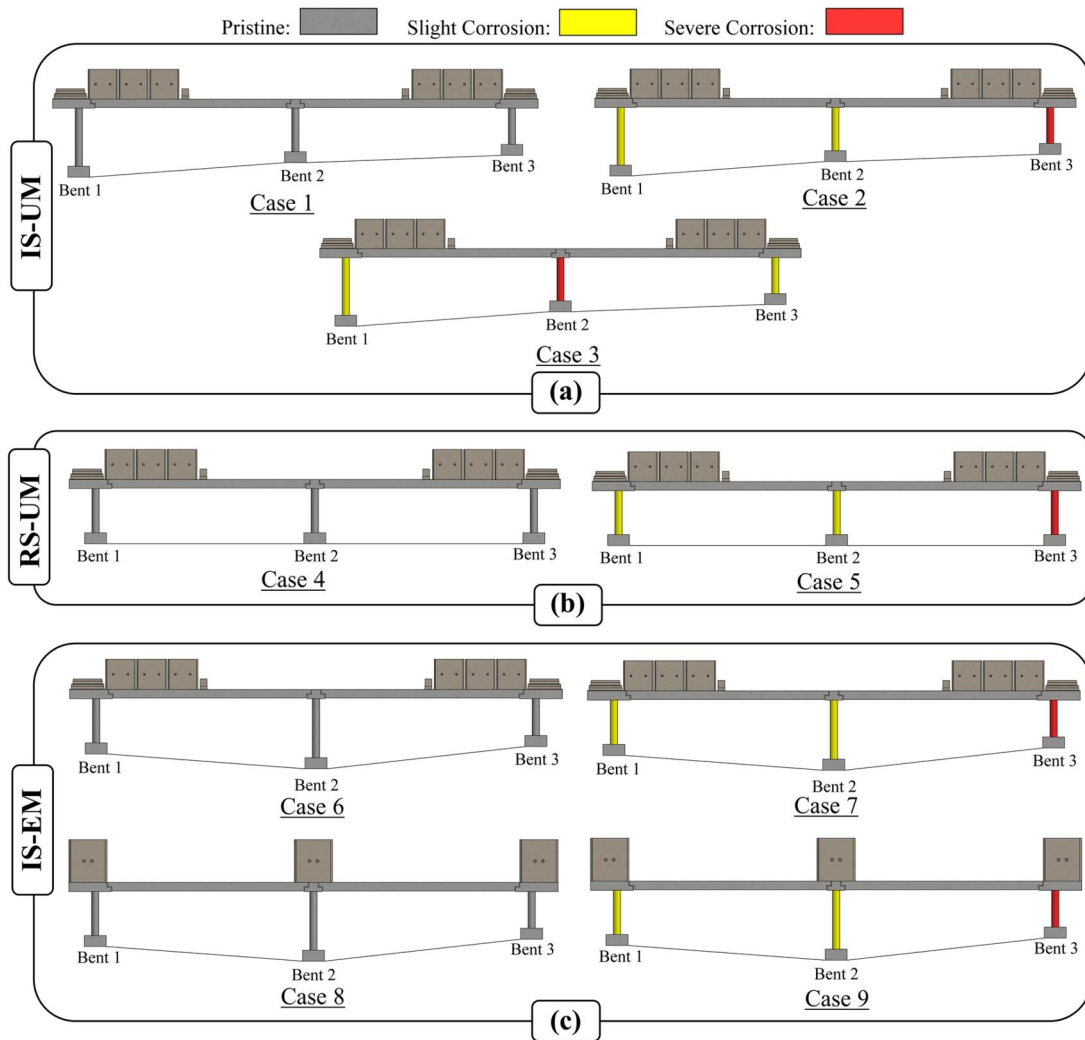


Figure 6. The hypothetical bridge layouts: (a) is-UM bridge, (b) RS-UM bridge and (c) IS-EM bridge.

Table 2. Characteristics of considered bridge layouts and cases.

Bridge label	Case No.	Mass distribution condition	Stiffness regularity condition	Corrosion level		
				Bent 1	Bent 2	Bent 3
IS-UM	1	Unequal	Irregular	Pristine	Pristine	Pristine
	2	Unequal	Irregular	Slight	Slight	Severe
	3	Unequal	Irregular	Slight	Severe	Slight
RS-UM	4	Unequal	Regular	Pristine	Pristine	Pristine
	5	Unequal	Regular	Slight	Slight	Severe
IS-EM	6	Unequal	Irregular	Pristine	Pristine	Pristine
	7	Unequal	Irregular	Slight	Slight	Severe
	8	Equal	Irregular	Pristine	Pristine	Pristine
	9	Equal	Irregular	Slight	Slight	Severe

corrosion where the piers in bent 3 are more corroded than piers in bent 1 and 2.

The third layout is labelled as IS-EM (Irregular Stiffness and Equal Mass distribution), which translates to irregular stiffness and equal mass distribution. Figure 6c shows the schematic view of this bridge. The geometry and height arrangement of different bents of this bridge are similar to the benchmark bridge. As discussed in Section 2.1, while the applied axial force ratio on top of all piers is equal, the effective seismic mass of each bent is not equal due to the configuration of super-imposed masses. This causes

bent 2 to experience the least inertia force among the bents, while bents 1 and 3 absorb approximately the same inertia forces. This unequal distribution of super-imposed mass raises a question on the influence of the distribution of inertial forces between different bents on the overall seismic behaviour of a RC bridge with irregular configuration. Therefore, this scenario is considered to compare the influence of spatially variable corrosion of piers on failure modes and seismic fragility of irregular RC bridge systems with equal/unequal inertia forces acting on each bent. In order to equally distribute inertial forces across the

bents, the summation of all the super-imposed masses (shown in Figure 1) is divided into six piers to have all the piers with equal mass portions. A summary of the different bridge layouts and considered cases are presented in Table 2.

4. Time-dependent local damage index

In order to develop time-dependent fragility curves for the proposed corrosion-damaged bridges, there is a need for time-dependent seismic damage limit states. The following section proposes a time-dependent local damage index that will be used in seismic fragility analyses of corrosion-damaged bridges in Sections 5.2.2, 5.3.2 and 5.4.2.

4.1. Dimensionless local damage index

Different damage metrics are defined in the literature to evaluate the vulnerability of corrosion-damaged RC bridge components (Hwang, Liu, & Chiu, 2001; Ramanathan, 2012). Here, the dimensionless local damage index proposed by Mergos and Kappos (2013), later extended by Afsar Dizaj and Kashani (2020) to incorporate the corrosion damage, is used to evaluate the seismic fragility of selected bridge layouts. This combined damage index accounts for the contribution of different sources of damage, including flexural damage, shear damage and bar-slip damage. The following equations present the formulation of the employed combined total damage index, λ_{tot} :

$$\lambda_{tot} = 1 - \lambda_{fl} \times \lambda_{sh} \times \lambda_{sl} \quad (6)$$

$$\lambda_{fl} = 1 - \left(\frac{\varphi_{max}}{\varphi_u} \right)^{1.35} \quad (7)$$

$$\lambda_{sh} = 1 - \left(\frac{\gamma_{max}}{\gamma_u} \right)^{0.8} \quad (8)$$

$$\lambda_{sl} = 1 - \left(\frac{\theta_{max}}{\theta_u} \right)^{0.95} \quad (9)$$

where λ_{fl} , λ_{sh} and λ_{sl} are the damage contribution due to flexural, shear and reinforcement slippage, respectively. Moreover, φ_u , γ_u and θ_u are the curvature capacity, ultimate shear strain capacity and fixed-end rotation capacity. Some studies consider the effects of cyclic loading in determining deformation capacities.

For instance, Akiyama, Frangopol, and Matsuzaki (2011) proposed an analytical method for quantifying the ductility of RC bridge piers associated with the buckling onset of corroded reinforcement. As an alternative approach, the deformation capacities (φ_u , γ_u and θ_u) can be obtained from the results of monotonic pushover analysis. Further details are available in (Mergos & Kappos, 2013; Afsar Dizaj & Kashani, 2020). The procedure provided by Afsar Dizaj and Kashani (2020) is implemented in this study to incorporate the adverse influence of corrosion on deformation capacities. Finally, φ_{max} , γ_{max} and θ_{max} are maximum curvatures, maximum shear strain and maximum reinforcement slip-page-induced rotation values, respectively.

It is important to note that the influence of cyclic loading is considered indirectly in the formulation of the employed damage index by calibrating the exponents of normalised deformations (φ_{max}/φ_u , λ_{max}/λ_u and θ_{max}/θ_u) against cyclic test results of RC columns with various failure modes (Mergos & Kappos, 2013). Moreover, as described in Section 2, the proposed finite element modelling technique simulates the degradation in the cyclic response of bridge piers due to the low-cycle fatigue degradation and inelastic buckling of reinforcement; both can affect structural response and impact maximum deformation values (φ_{max} , γ_{max} and θ_{max}). Using the calculated total damage index, the physical damage states of RC bridge piers can be categorised into three levels: minor, moderate and severe. This

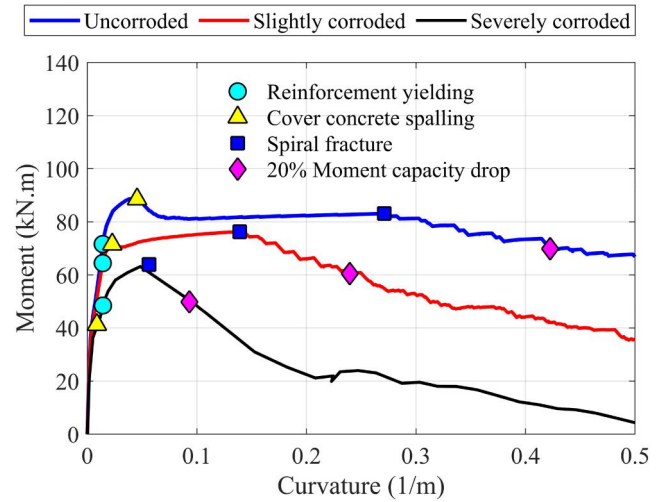


Figure 7. Moment-curvature analysis results of the medium-height bent for different corrosion levels.

Table 3. Definition of different damage states for flexural, shear and bond damage mechanisms (Mergos & Kappos, 2013).

Damage level	Flexural damage	Shear damage	Bond damage	Damage index (λ_{tot})
Minor	Flexural cracks (<2 mm), limited yielding, no spalling	Hairline minor shear cracks (<0.5 mm)	Fixed-end cracks (<2 mm). Hairline-visible bond cracks in parts of the lap splices	0.0–0.20
Moderate	Spalling of cover concrete	Moderate shear cracking (>0.5 mm)	Fixed-end cracks (>2 mm). Moderate bond cracking in parts of the lap splices	0.20–0.50
Severe	Rebar buckling, core concrete disintegration, fracture of tensile reinforcement, yielding or fracture of transverse reinforcement because of core expansion	Sever shear cracking (>1 mm), stirrup yielding or fracture	Major fixed-end cracks indicating reinforcement pullout. Severe bond cracking along the full length of the lap splices. Spalling of cover surrounding lap-spliced bars	0.50–1.00

classification of damage states and the definition of each damage state are provided in Table 3.

4.2. Monotonic pushover analysis

As discussed in Section 4.1, the ultimate deformation capacity values of piers are derived from monotonic pushover analysis results of bridge bents. To conduct pushover analysis, each bridge bent with a tributary axial load ratio of its

columns is modelled separately and subjected to lateral displacement control loading to conduct the pushover analysis. Nine pushover analyses were performed considering three bents each with three different corrosion levels (uncorroded, slightly corroded and severely corroded). The P-delta effects due to the compressive axial gravity load are considered in the analyses. Moreover, the material and geometrical properties of bridge piers are updated for the hypothetical corrosion levels. Additionally, the material responses of concrete and steel at the critical region are recorded during each analysis.

Figure 7 depicts the moment-curvature analysis results of the medium-height bent with different corrosion levels. In this figure, the associated curvature with the onset of longitudinal reinforcement yielding, cover concrete spalling, spiral fracture (which corresponds to core concrete crushing) and 20% drop in moment capacity of each pier with different corrosion levels are mapped on each curve. According to the definition provided in references Mergos and Kappos (2013) and Afsar Dizaj and Kashani (2020), the least

Table 4. Deformation capacities derived from the pushover analysis results.

Corrosion level	Bent	$\phi u(1/m)$	$\theta u(\text{rad})$	γu
Pristine	Short	0.2734	0.0619	0.0129
	Medium-Height	0.2741	0.0617	0.0128
	Tall	0.2768	0.0599	0.0128
Slight	Short	0.1412	0.0594	0.0097
	Medium-Height	0.1419	0.0593	0.0097
	Tall	0.1439	0.0590	0.0096
Severe	Short	0.0602	0.0594	0.0049
	Medium-Height	0.0608	0.0593	0.0049
	Tall	0.0626	0.0590	0.0049

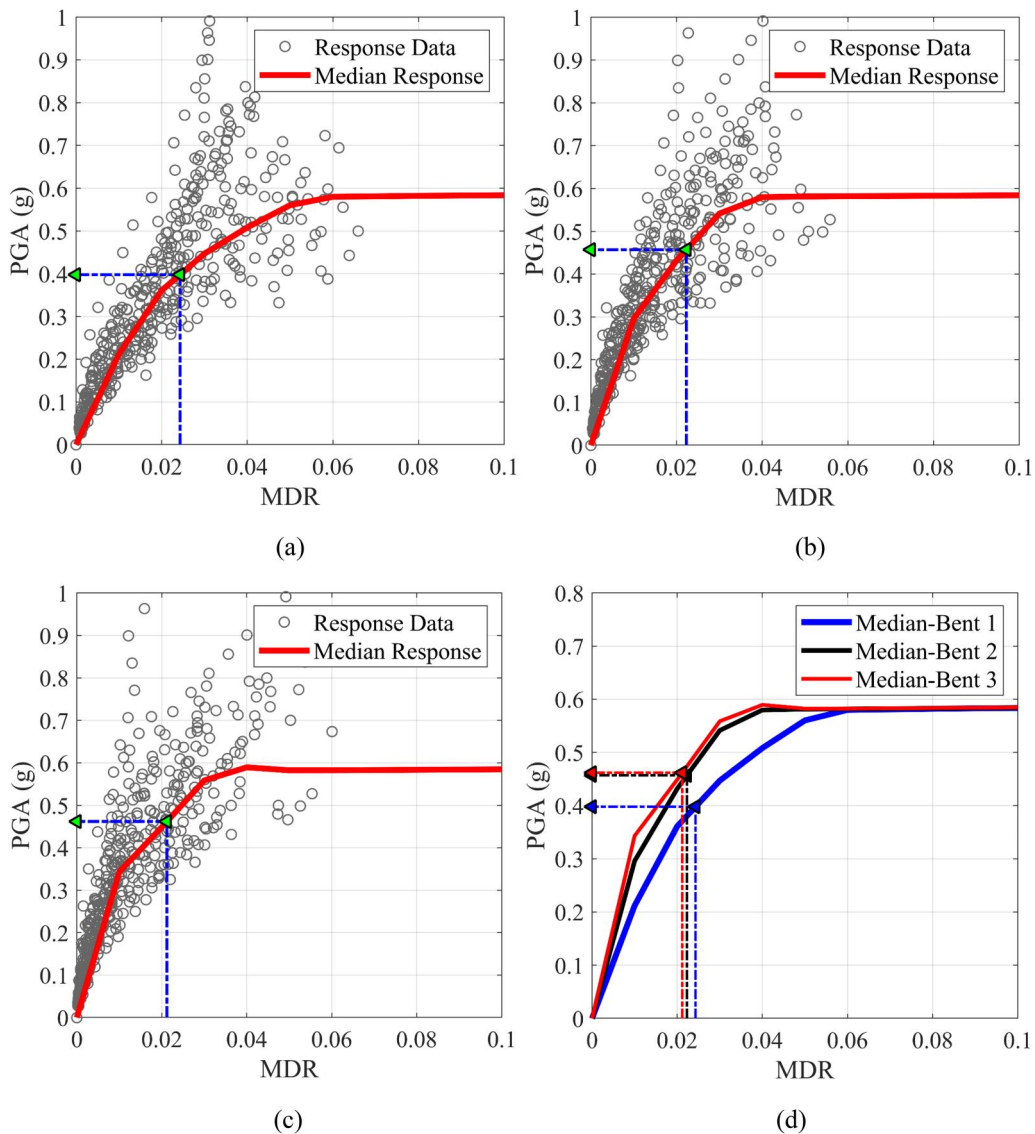


Figure 8. IDA results of case 1: (a) bent 1, (b) bent 2, (c) bent 3 and (d) median curves.

amount between associated curvature with the core concrete crushing, fracture of longitudinal reinforcement, and 20% capacity drop is considered as the curvature capacity, φ_u . The details on calculating the other two ultimate deformation capacities (γ_u and θ_u) are available in Afsar Dizaj and Kashani (2020).

It is noteworthy to mention that because all the bridge piers of the studied piers are flexural govern components, the contribution of shear damage to the total damage index is negligible, and the main contribution comes from the flexural damage (i.e., λ_f). In Table 4, the calculated values of ultimate deformation capacities are tabulated for different

bents and corrosion levels considered in the current study. As seen in this table, the value of ultimate deformations decreases significantly as the corrosion level increases.

5. Incremental dynamic and seismic fragility analyses results and discussion

Incremental Dynamic Analysis (IDA) is an efficient approach to tracking the nonlinear dynamic behaviour of structures in a wide range of different earthquake intensities. In this section, this approach is employed to study the influence of spatially variable corrosion of piers on seismic behaviour and fragility of the case-study irregular RC bridges.

5.1. Ground motion selection

Selecting a sufficient number of ground motion records is fundamental to conducting IDA. The selected record set

Table 5. Median PGA values associated with failure of each bent in IS-UM bridges.

Case No.	Bent 1	Bent 2	Bent 3
Case 1	0.40 g	0.46 g	0.46 g
Case 2	0.24 g	0.28 g	0.20 g
Case 3	0.25 g	0.22 g	0.30 g

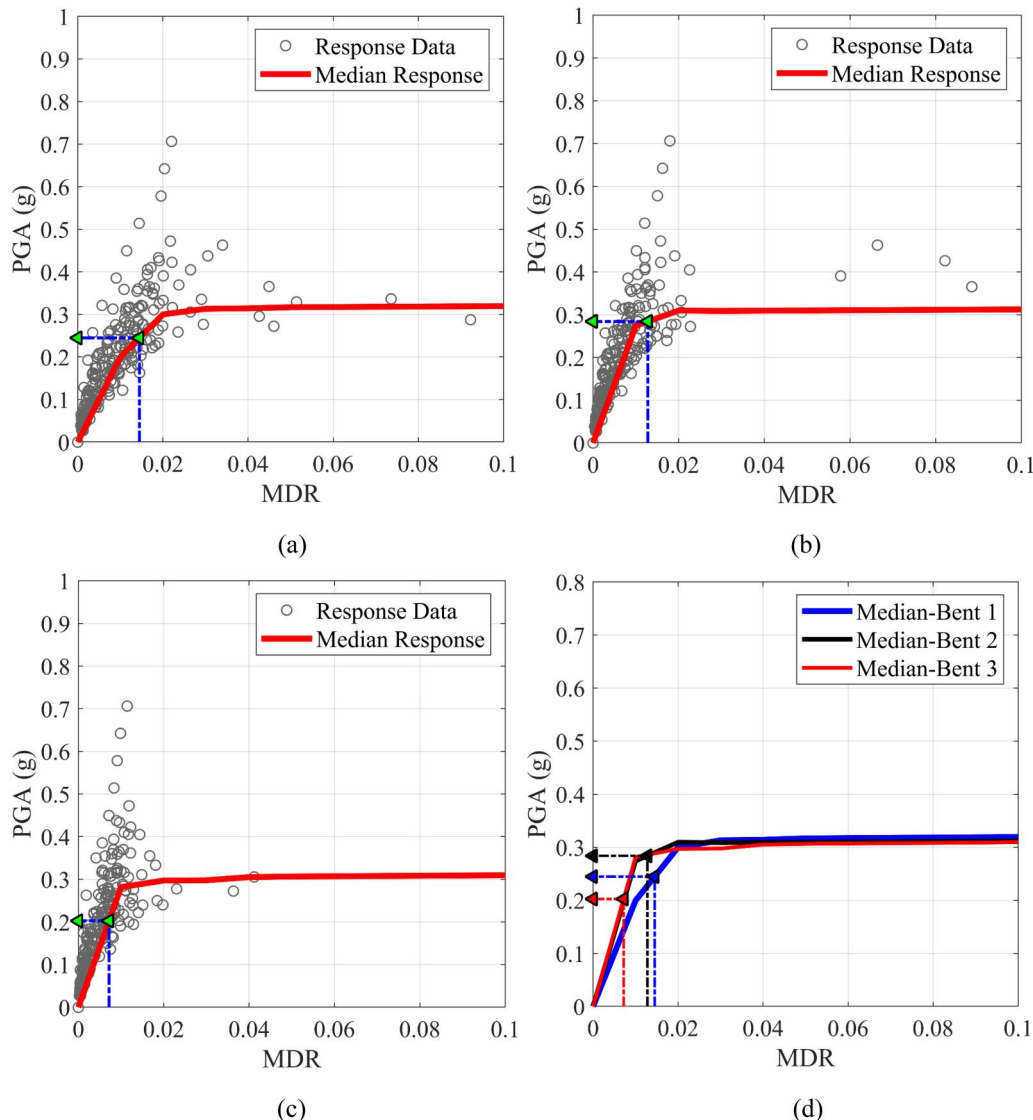


Figure 9. IDA results of case 2: (a) bent 1, (b) bent 2, (c) bent 3 and (d) median curves.

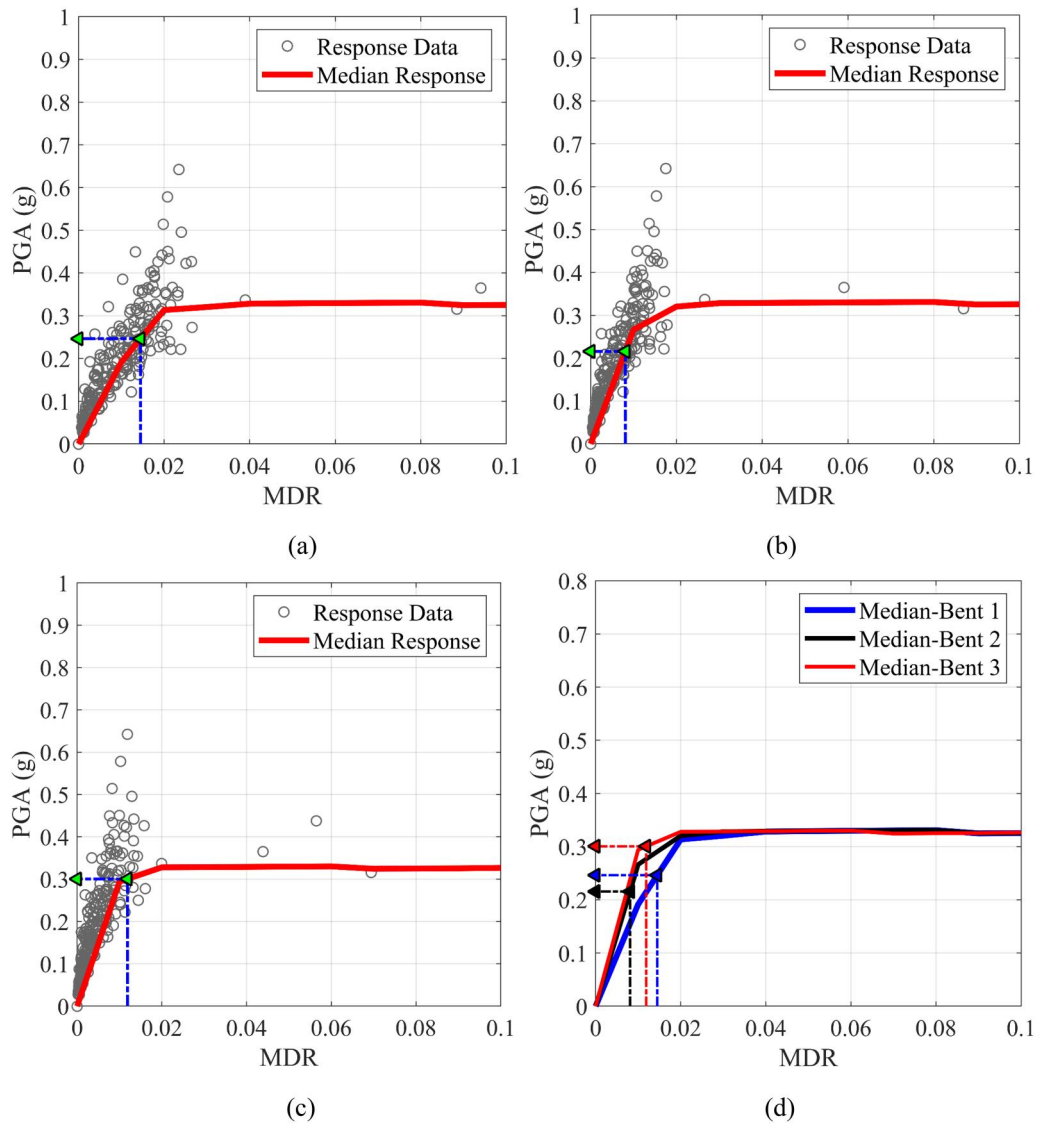


Figure 10. IDA results of case 3: (a) bent 1, (b) bent 2, (c) bent 3 and (d) median curves.

should cover a wide range of earthquake intensities to consider the uncertainty associated with the record-to-record variability. Here, a set of 32 ground motions (16 record pairs) are selected from the far-field records provided in FEMA P695,695 (2009). Here, PGA is considered an earthquake record intensity measure (IM). To carry out IDAs, the selected ground motions with incrementally scaled-up IMs are applied to the bridge structure, and the maximum drift ratio (MDR) of each bent associated with each IM is considered a damage measure (DM).

5.2. Impact of spatially variable corrosion on seismic performance of IS-UM bridge

5.2.1. Nonlinear dynamic response

Figure 8 shows the IDA results of case 1. Each circular marker in Figures 8a–c represents a (MDR, PGA) pair obtained from every single time-history analysis with a given input IM, and its corresponding induced DM. The

median IDA curves are plotted for each bent to summarise the IDA output. Additionally, the drift ratio associated with the onset of spiral fracture (core concrete crushing) is plotted by a vertical dashed line, showing the failure threshold of each bent. The intersection of this line with the median IDA curve extracts the median PGA corresponding to the failure of each bent. The median PGA values associated with the failure of different bents in IS-UM bridge layouts are summarised in Table 5.

A comparison between the median IDA response of all bents in case 1 (Figure 8d) shows that the median failure of bent 1 (supported on tallest piers) occurs at approximately $PGA = 0.4$ g, whereas the other bents fail at about $PGA = 0.46$ g. This gives valuable information on the failure sequence of unequal-height bents in case 1.

Figure 9 displays the IDA results of case 2. As results show, the plateau response of bents reaches much lower IMs than the uncorroded bridge (Figure 8), indicating a significant reduction in their capacity due to the corrosion-

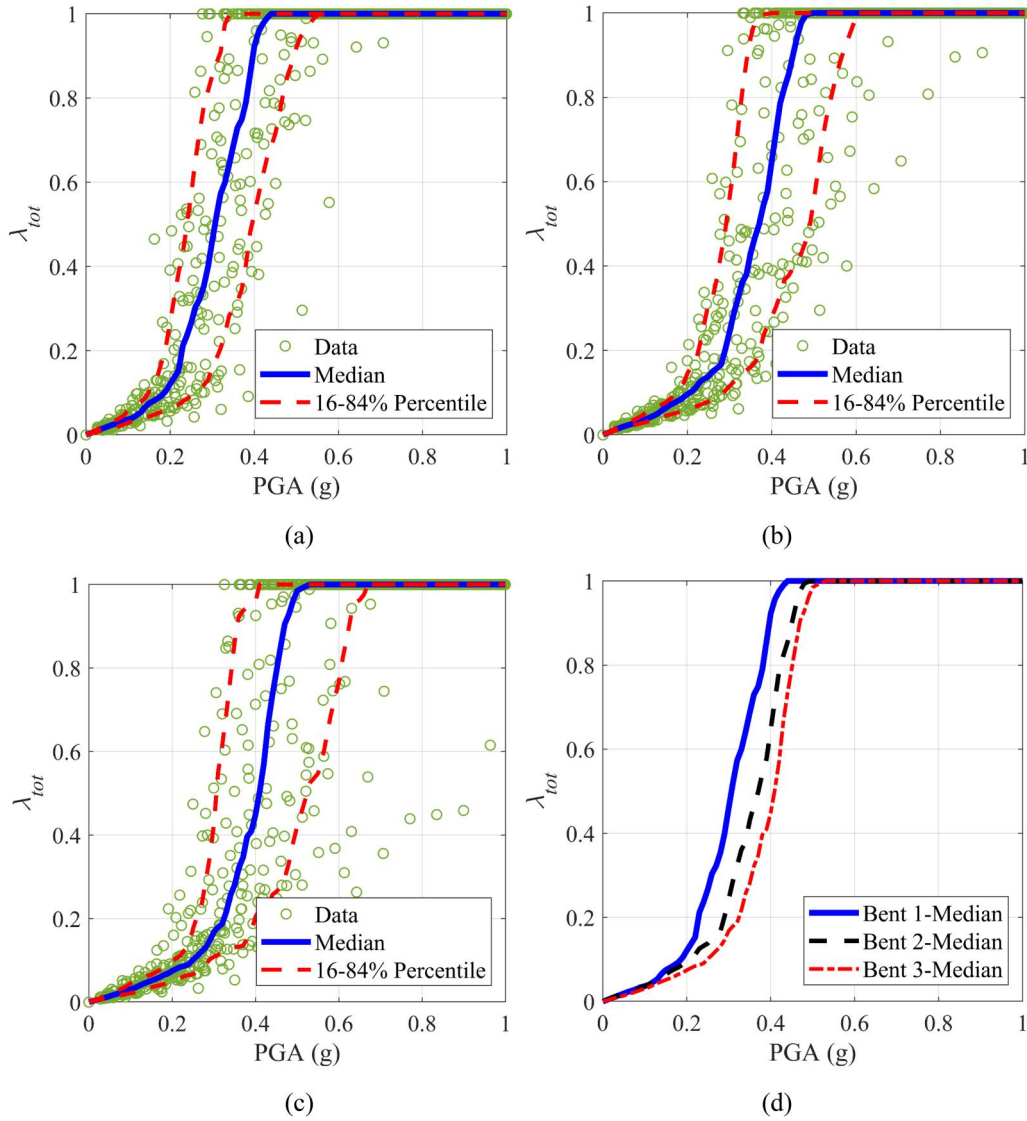


Figure 11. Progression of local damage in case 1: (a) bent 1, (b) bent 2, (c) bent 3 and (d) median curves.

induced damage. Moreover, Figure 9d shows that the asymmetric corrosion of piers changes the failure pattern of bents, where the severely corroded piers of bent 3 fail earlier than other bents. This is due to the significant reduction in the volumetric ratio of corrosion-damaged spirals, which results in the premature failure of core concrete. Similarly, Figure 10d indicates that medium-height piers in the middle bent (bent 2) are critical bridge piers in case 3 due to their relatively more significant corrosion damages. Figure 10d shows that the severely corroded bent 2 fails at approximately median IM = 0.22g, whereas bent 1 and bent 3 fail at about IM = 0.25g and IM = 0.3g, respectively.

The above discussion on the IDA response of the considered IS-UM bridge shows the notable influence of spatially variable corrosion of piers on the nonlinear dynamic and failure sequence of irregular bridge piers. However, the IDA results in terms of PGA-MDR response do not provide any information on the progression of damage at the local scale. For this reason, the dimensionless local damage index (Section 4.1) is used to investigate the extent of damage at the material scale. To this end, for each IM, the values of

φ_{max} , γ_{max} and θ_{max} are extracted, and then, using Eq. (6), the value of λ_{tot} is calculated. Using the formulation given in Eq. (6), the points of $\lambda_{tot}=1$ will correspond to the failure at the local scale.

Figure 11 shows the variation of λ_{tot} against PGA for each bent. The median and 16–84% percentile curves are plotted for each bent to summarise the results. Moreover, in Figure 11d, the median curves of all bents are compared. As Figure 11d shows, beyond PGA = 0.2g, the local damage index of bent 1 is more significant for each IM than bent 2 and bent 3. For instance, for PGA = 0.4g, the median value of λ_{tot} for bent 1, bent 2 and bent 3 are approximately 0.9, 0.6 and 0.45, respectively. Moreover, the median failure point of bent 1 takes place before the other bents. This conclusion is consistent with the results shown in Figure 8d.

The progression of local damage against the intensity level of earthquakes is analogously plotted in Figures 12 and 13 for case 2 and case 3, respectively. Figure 12 shows that a slight increase in the PGA of input earthquakes results in a sharp rise in the amount of λ_{tot} . Such steep progression of damage is related to deteriorated capacity and ductility of

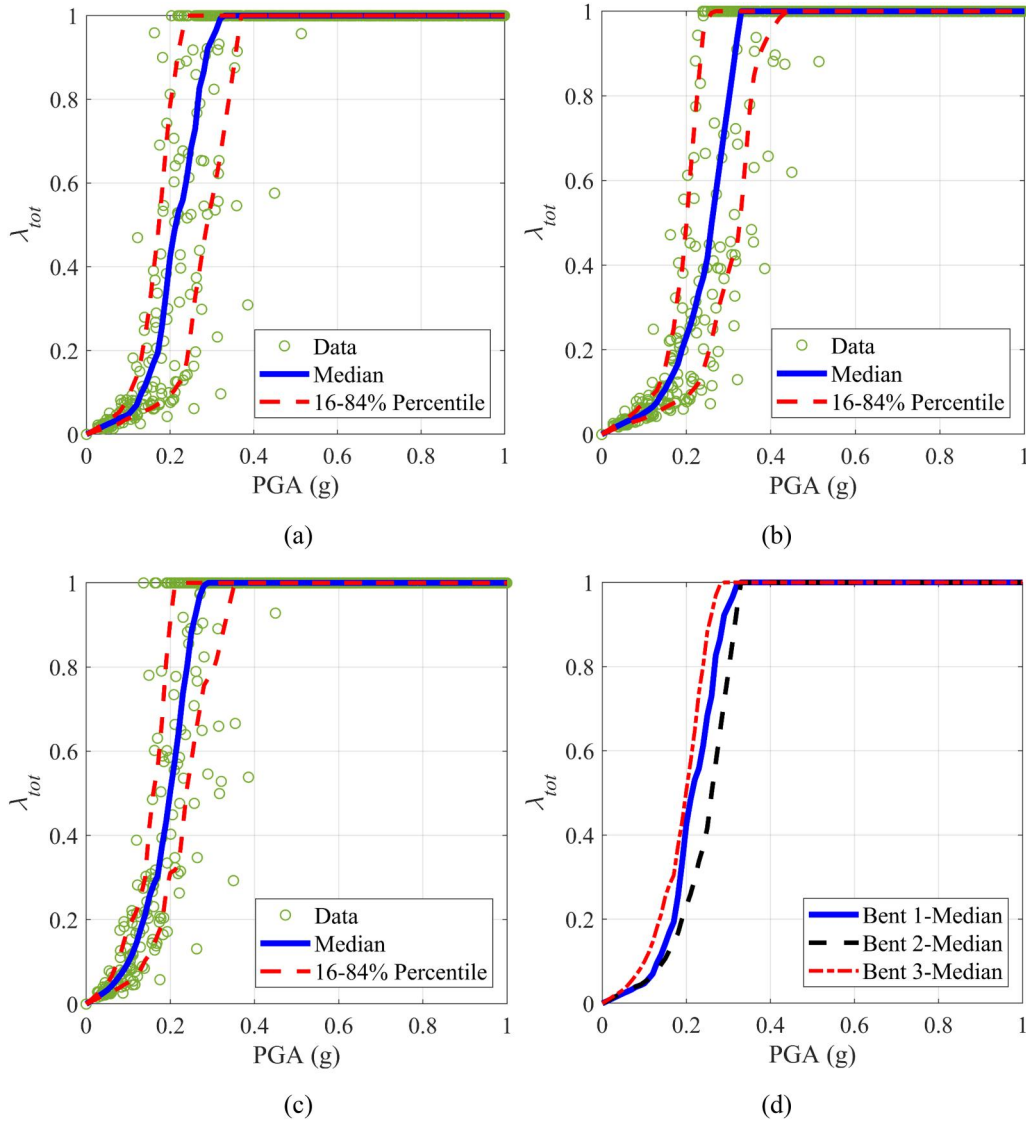


Figure 12. Progression of local damage in case 2: (a) bent 1, (b) bent 2, (c) bent 3 and (d) median curves.

corroded bridge piers. Figure 12d indicates that the collapse of bridge case 2 is governed by premature failure of excessively corroded short piers located in bent 3. However, as Figure 13d shows, the spatially variable corrosion of piers causes near-concurrent failure of bent 1 and bent 2 in bridge case 3. Also, Figure 13d shows that, up to $PGA=0.2g$, bent 3 supported on shorter piers does not experience significant damage at the material scale since the damage is mainly accumulated in bent 1 and bent 2. However, after the simultaneous failure of these two bents, the local damage level increases rapidly in bent 3, causing its failure just after the failure of bent 1 and bent 2. The above discussion shows that investigating damage at the material scale provides a more efficient and deeper insight into the failure morphology of irregular bridges with spatially variable corrosion of piers.

5.2.2. Seismic fragility analysis

To quantify the impact of spatially variable corrosion on the failure probability of hypothetical IS-UM bridge cases,

fragility curves are developed for each bent. The fragility curves are developed using a lognormal distribution function as:

$$P[SDI \geq LS_i | IM] = 1 - \Phi\left(\frac{\ln(LS_i) - \ln(m_{SDI|IM})}{\beta_{SDI|IM}}\right) \quad (10)$$

where SDI denotes the structural damage index, LS_i is the i^{th} damage limit state conditioned on the value of IM , and $m_{SDI|IM}$ and $\beta_{SDI|IM}$ are the median and standard deviation of SDI , respectively, which can be obtained using:

$$\ln(m_{SDI|IM}) = \frac{\sum_{i=1}^n \ln(SDI)}{n} \quad (11)$$

$$\beta_{SDI|IM} = \sqrt{\frac{\sum_{i=1}^n (\ln(SDI) - \ln(m_{SDI|IM}))^2}{n-1}} \quad (12)$$

Here, λ_{tot} is considered as SDI , and the median value of severe damage level (which corresponds to $\lambda_{tot}=0.75$ (Mergos and Kappos (2013)) is adopted as the collapse limit state (Salami, Afsar Dizaj, & Kashani, 2021) to plot the

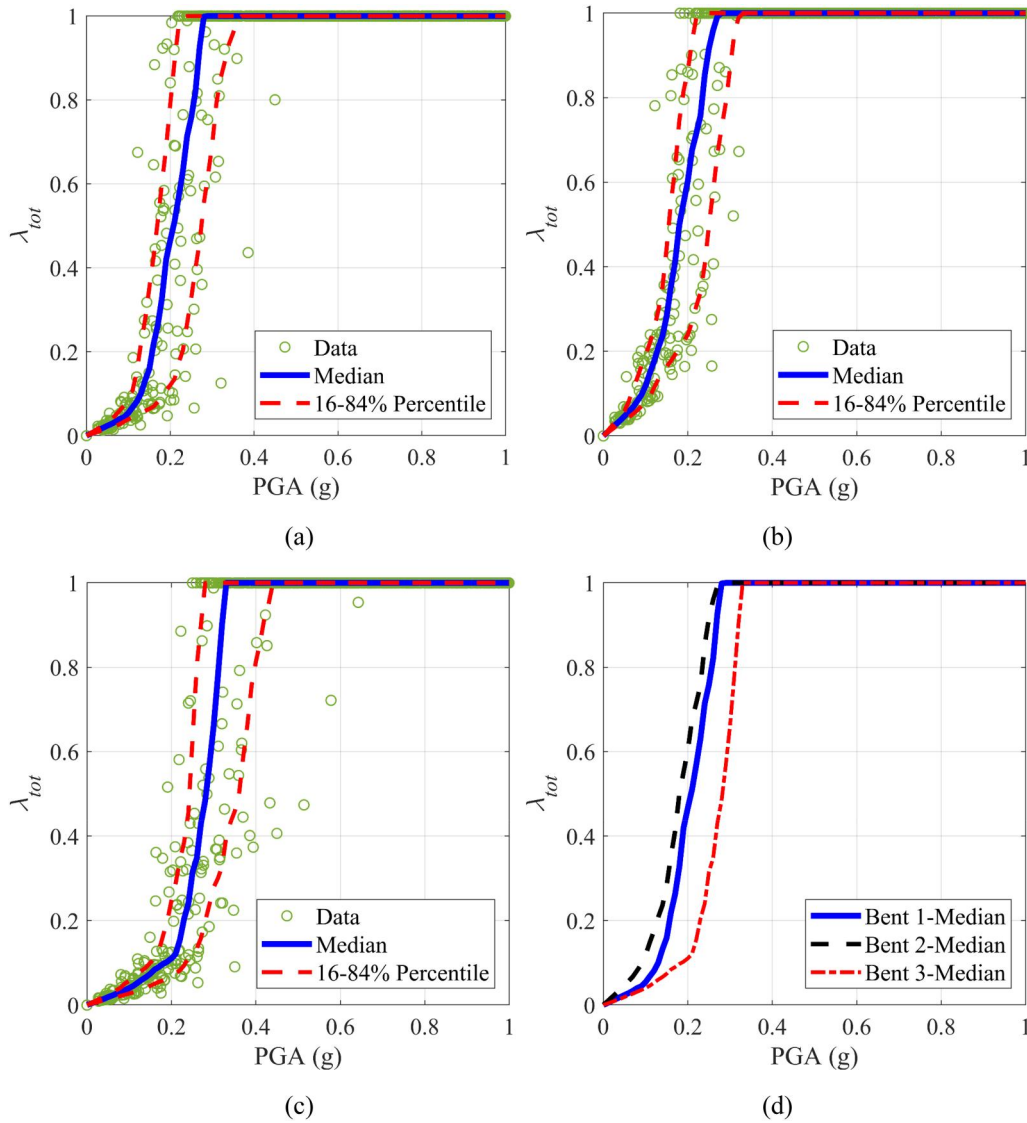


Figure 13. Progression of local damage in case 3: (a) bent 1, (b) bent 2, (c) bent 3 and (d) median curves.

fragility curves. Figure 14 compares the fragility curves of all bents in each case. As Figure 14a shows, for a given IM, the failure probability of bent 1 is greater than other bents. For example, for $PGA = 0.6g$, the failure probability of bent 1 is approximately 82%, whereas it is 70% and 60% for bent 2 and bent 3, respectively. However, Figure 14b shows that in case 2, the higher corrosion level of bent 3 leads to a drastic increase in the failure probability of this bent beyond $PGA = 0.2g$. Similarly, in case 3, the spatially variable corrosion of piers significantly affects the fragility of piers, where the middle bent with the greater level of corrosion becomes more vulnerable than other bents.

5.3. Impact of spatially variable corrosion on seismic performance of RS-UM bridge

5.3.1. Nonlinear dynamic response

Figure 15 displays the median IDA results of RS-UM bridge configuration on global and local scales. As expected, median IDA responses of all bents in the uncorroded regular bridge

(case 4) are the same (Figure 15a). It should be noted that the negligible slight differences in IDA curves and median failure points arise from the unequal super-imposed mass distribution, which triggers unbalanced inertia forces on each bent. However, as shown in Figure 15b, the spatially variable corrosion of piers changes the median IDA response of bents, where the median failure criteria of severely corroded bent 3 reaches approximately $PGA = 0.18g$, whereas that of the other two bents occurs at about $0.24g$. The PGA values associated with the onset of failure of bents in case 4 and case 5 are provided in Table 6. Moreover, the same trend can be observed in the damage progression at the material scale (Figures 15c, d), where bent 3 experiences higher local damage than other bents for a given IM.

It can be determined from the above discussion that the spatially variable corrosion of bridge piers can trigger unbalanced seismic demand in different bents of a multi-span regular RC bridge. Depending on the spatially variable corrosion scenario, bridge geometry and intensity of the seismic event, the irregularity in the distribution of seismic

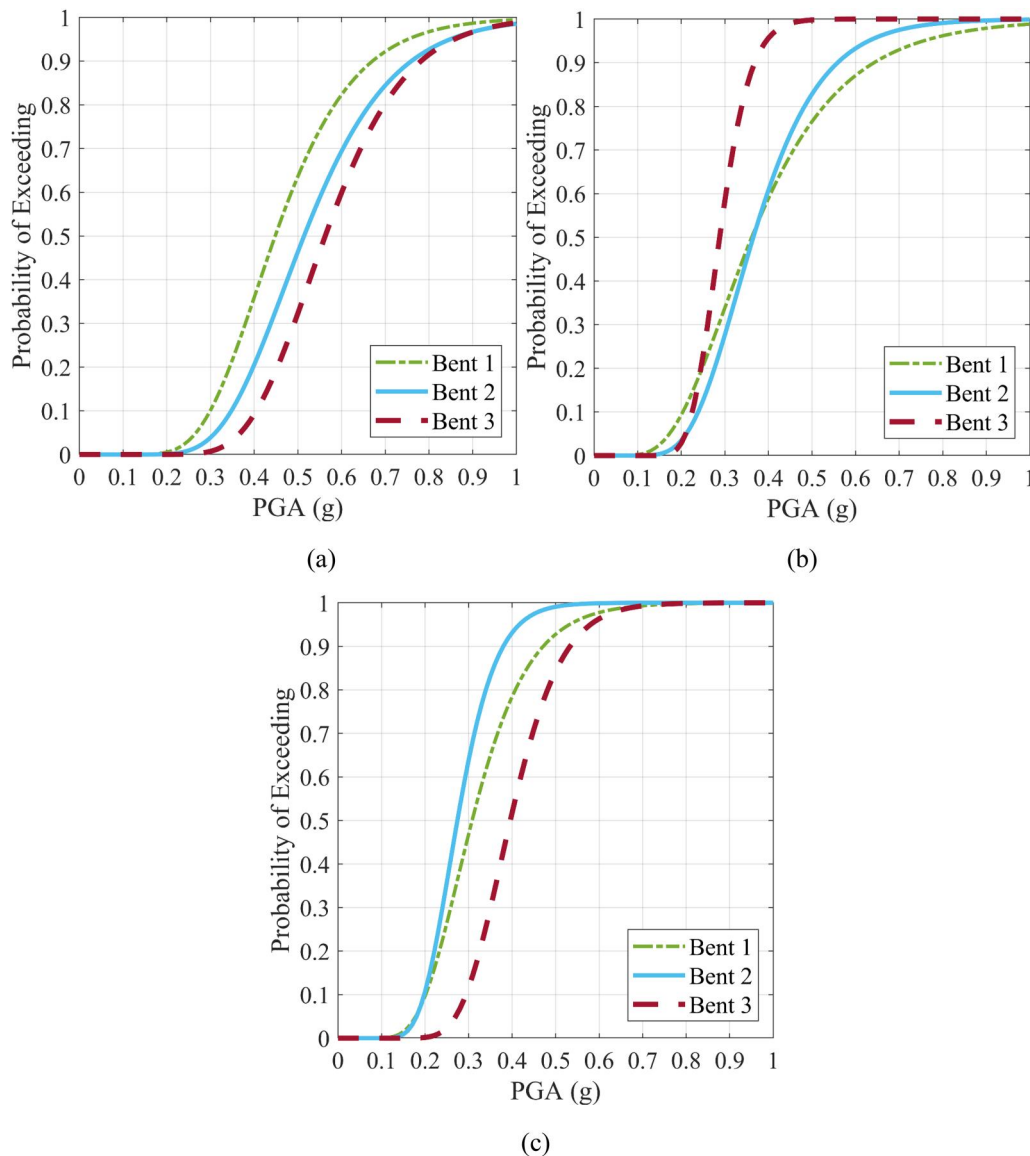


Figure 14. Fragility curves of IS-UM bridge specimen: (a) case 1, (b) case 2 and (c) case 3.

ductility demands due to the spatially variable corrosion of bridge piers might even be intensified. Therefore, the spatially variable corrosion of piers should be considered as another source of irregularity in multi-span RC bridges. Nevertheless, further studies considering multiple bridge configurations and corrosion scenarios are necessary to profoundly investigate the unbalanced seismic behaviour of spatially variable corroded RC bridges.

5.3.2. Seismic fragility analysis

In Figure 16, the collapse fragility curves of equal-height bents are compared. As expected, all bents in case 4 have the same probability of failure for varied IMs (Figure 16a). However, as Figure 16b shows, the spatially variable corrosion of bridge piers makes the fragility curve of severely corroded bent 3 more fragile than other bents. For instance, when $PGA = 0.4g$, the failure probability of bent 3 is increased by approximately 40% compared to that of bent 1 and bent 2.

5.4. Impact of spatially variable corrosion on seismic performance of IS-EM bridge

5.4.1. Nonlinear dynamic response

Figure 17 depicts the influence of equal/unequal distribution of super-imposed masses between the bents of varying height on the median IDA response of IS-EM bridge configuration. Comparing Figure 17a,b, it can be concluded that the irregular distribution of super-imposed masses considered in this study does not have a significant impact on the overall median response of uncorroded irregular bridge layout (case 6). Likewise, the failure sequence and the corresponding IM at the failure of all bents are not affected by the equal distribution of masses (Figure 17b).

However, a comparison between Figure 17c and Figure 17d indicates that for the spatially variable corroded bridge (case 7), the equal distribution of superstructure masses (in case 9) has a considerable impact on median IDA curves. Particularly, Figure 17d shows that the PGA at the onset of failure of all bents is shifted above, showing the lower

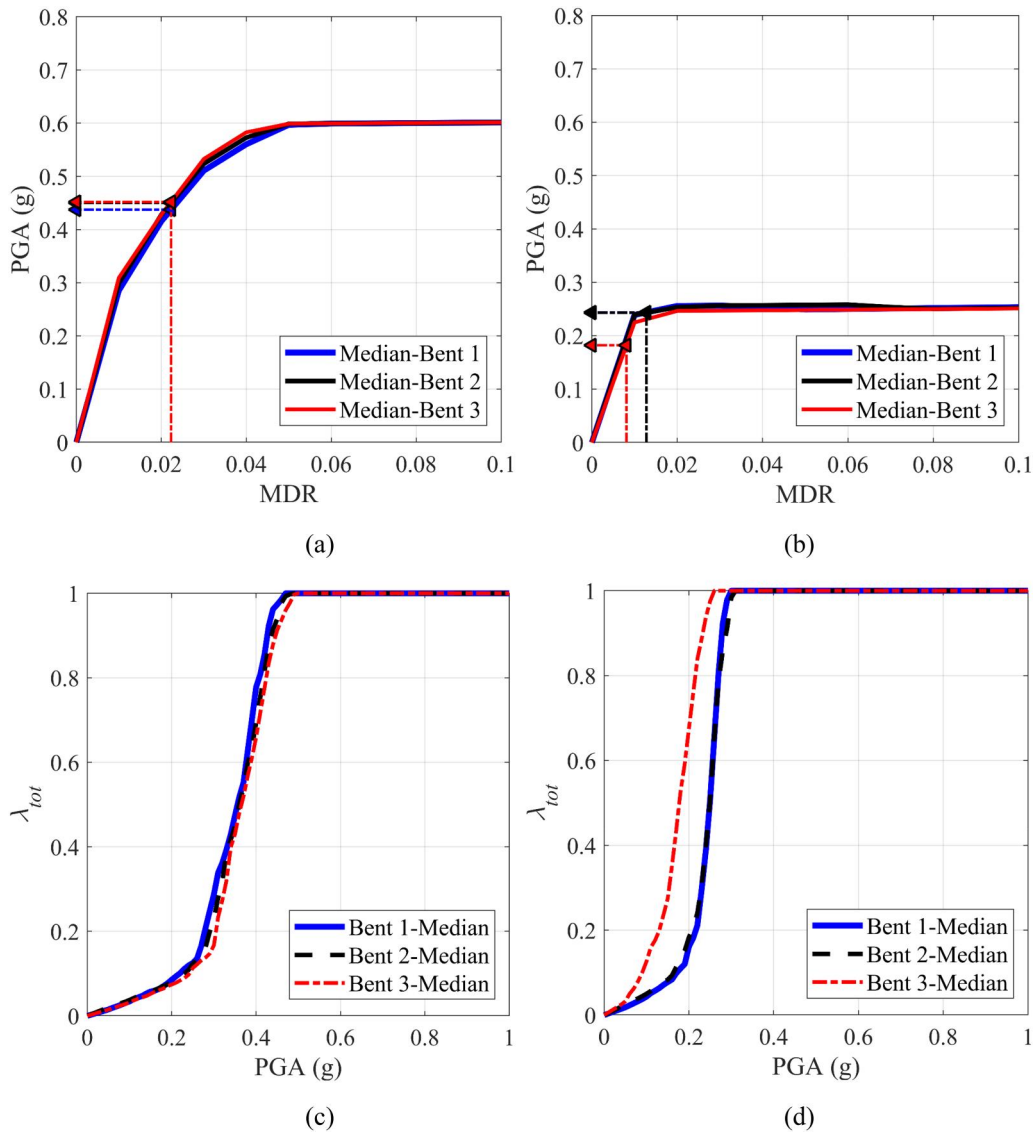


Figure 15. Median IDA results and variation of local damage index in RS-UM bridge layout: case 4 (a and c) and case 5 (b and d).

Table 6. Median PGA values associated with failure of each bent in RS-UM bridges.

Case No.	Bent 1	Bent 2	Bent 3
Case 4	0.44 g	0.45 g	0.45 g
Case 5	0.24 g	0.24 g	0.18 g

failure probability of bents in case 9 compared to case 7. This implies that the unbalanced inertia forces due to the unequal acting tributary mass on each bent have a more adverse influence on the nonlinear dynamic behaviour of spatially variable corroded irregular bridges. The PGA values associated with the failure of bents in cases 6 to 9 are tabulated in Table 7.

5.4.2. Seismic fragility analysis

To quantitatively compare the failure probability of bents for different mass distribution conditions, in Figure 18, the collapse fragility curves are developed for the considered IS-EM bridge scenarios. This figure shows that the regular distribution of mass decreases the failure probability of bridge

bents for all the IS-EM bridge cases. For instance, as Figure 18b shows, for $PGA = 0.5g$, the failure probability of bent 1, bent 2 and bent 3 are approximately 50%, 16% and 18%, respectively. These values show about 37%, 47% and 57% reduction in failure probability of bent 1, bent 2 and bent 3, compared to Figure 18a. However, comparing Figure 18d with Figure 18c reveals that in spatially variable corroded bridge case 9, where the stiffer piers of bent 3 are highly corroded, the regular distribution of superstructure masses has a more considerable impact on the failure probability of middle bent than others.

For example, for $PGA = 0.5g$, while the failure probability of bent 2 shows approximately 57% reduction compared to case 7 (Figure 18c), this reduction is about 20% and 16% for bent 1 bent 3, respectively. This is because in case 7 where the piers of bent 3 are severely corroded, the irregular distribution of super-imposed masses applies more inertial forces on bent 1 and bent 3. Consequently, a slight reduction in collapse probability of bent 3 due to equal distribution of inertia forces notably reduces the failure probability of adjacent bent, i.e., bent 2. It is worth highlighting that,

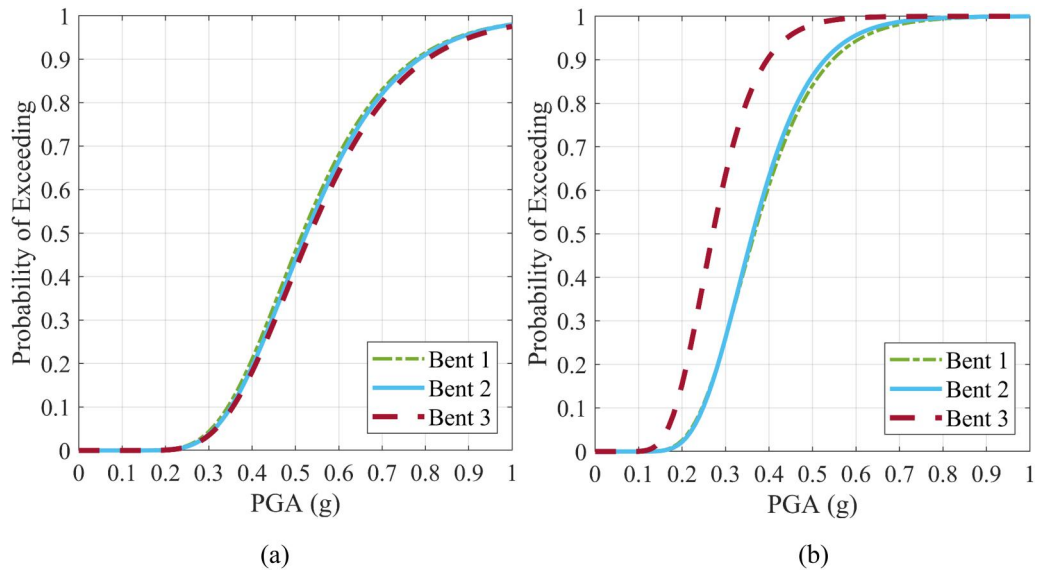


Figure 16. Fragility curves of RS-UM bridge specimen: (a) case 4 and (b) case 5.

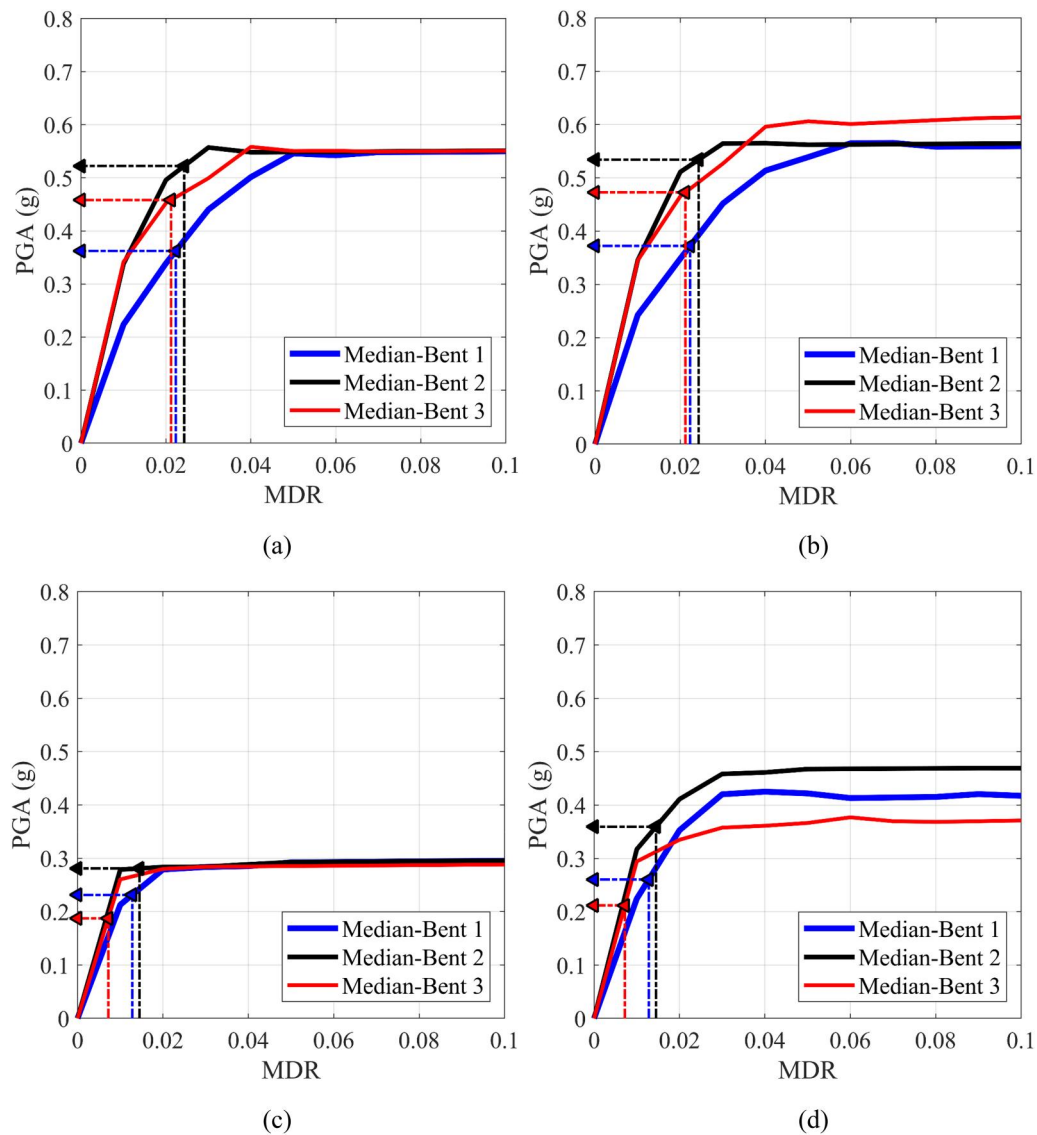


Figure 17. Median IDA results of IS-EM bridge layout: (a) case 6, (b) case 8, (c) case 7 and (d) case 9.

due to the severe reduction in capacity and ductility of the extremely corroded short piers, the equal/unequal distribution of super-imposed masses does not considerably affect the failure probability of these piers.

6. Conclusions

This article investigated the influence of spatially variable corrosion of bridge piers on the nonlinear dynamic and seismic fragility of multi-span RC bridges. To this end, an advanced three-dimensional nonlinear finite element model was developed and validated accurately by large-scale shake

table test results. Subsequently, three groups of bridge layouts labelled as IS-UM, RS-UM and IS-EM (nine cases in total) were considered to study the influence of substructure stiffness irregularity, spatially variable corrosion of piers and unbalanced inertia forces (unequal mass distribution) acting on piers of varying heights, on seismic fragility of such bridges. Finally, an advanced time-dependent local damage index was employed to investigate the influence of spatial variability of corrosion of piers on nonlinear dynamic behaviour, progression of damage in the local scale, failure sequence and time-dependent seismic fragility of considered regular and irregular ageing concrete bridges.

The following key conclusions can be drawn from the obtained results:

- Spatially variable bridge piers corrosion significantly affects the nonlinear dynamic behaviour and failure sequence of bents in multi-span RC bridges with substructure irregularity. Moreover, the analysis outcomes show that spatial variability of corrosion of piers

Table 7. Median PGA values associated with failure of each bent in IS-EM bridges.

Case No.	Bent 1	Bent 2	Bent 3
Case 6	0.36 g	0.52 g	0.46 g
Case 7	0.23 g	0.28 g	0.19 g
Case 8	0.37 g	0.53 g	0.47 g
Case 9	0.26 g	0.36 g	0.21 g

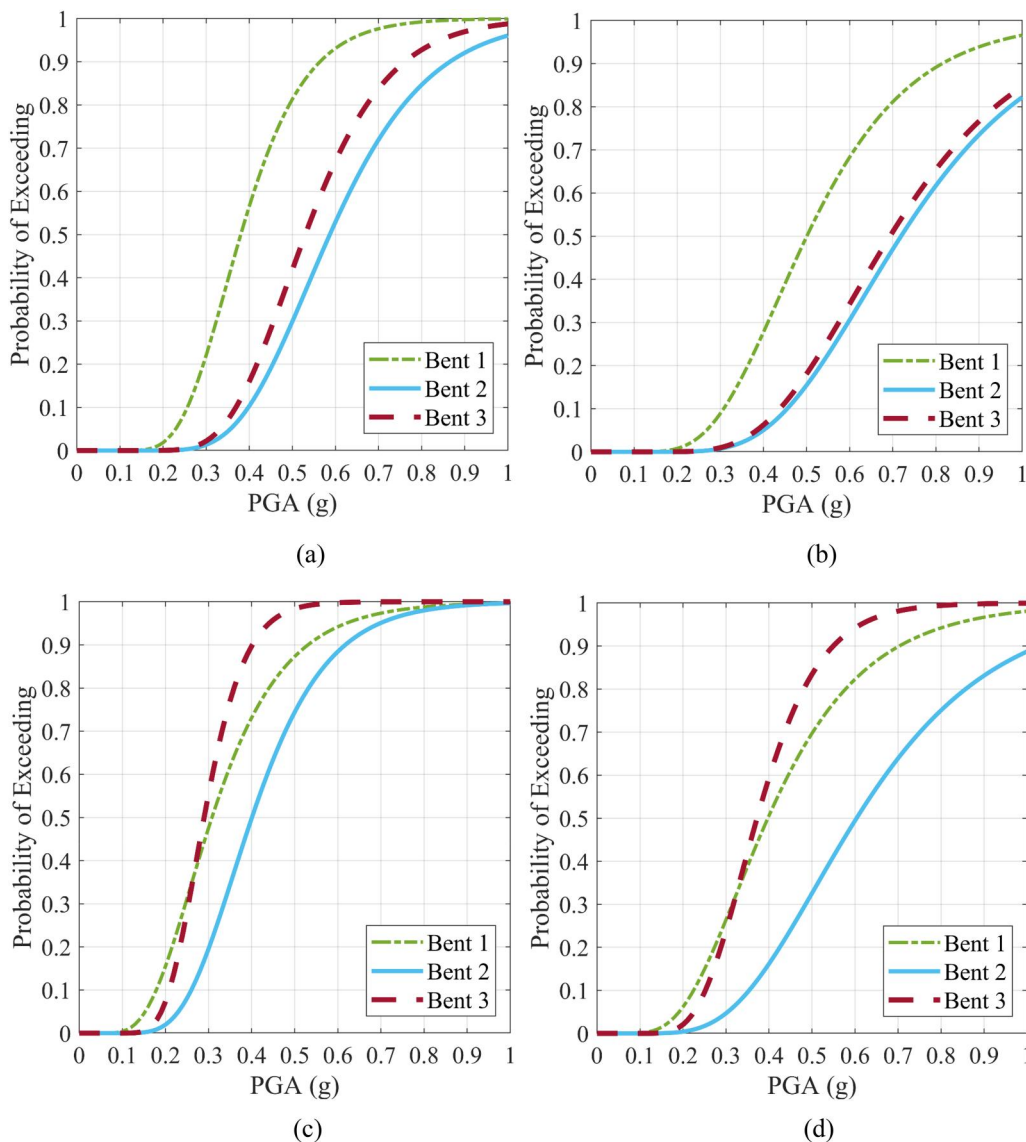


Figure 18. Fragility curves of IS-EM bridge cases: (a) case 6, (b) case 8, (c) case 7 and (d) case 9.

significantly affects the failure probability of different bents in an irregular multi-span RC bridge. This is because piers with greater corrosion damage experience a significant reduction in confinement level, leading to their premature crushing and affecting the ductility demand distribution in other bents.

- The spatially variable corrosion of piers significantly affects the nonlinear dynamic behaviour and failure sequence of equal-height piers in multi-span RC bridges (regular bridges). This implies that the structural behaviour of a regular multi-span RC bridge subject to spatially variable corrosion of piers is qualitatively analogous to a bridge with substructure irregularity. Moreover, the unbalanced distribution of seismic ductility demands in such bridges might be further pronounced considering different corrosion damage scenarios, bridge geometries and earthquake intensities.
- The irregular distribution of inertia forces due to the non-uniform distribution of super-imposed masses has a relatively significant impact on the median IDA response of spatially variable corroded irregular RC bridges. However, the unequal distribution of super-imposed masses does not significantly influence the overall median response of the uncorroded irregular bridge layout. This is because, in a spatially variable corroded bridge, a pier with a more significant corrosion level determines the collapse of the structure. Therefore, the collapse probability of such piers is highly sensitive to their tributary inertia forces, and a slight change in their failure probability will significantly affect the collapse probability of the other piers with lower corrosion levels.

The results/conclusions are valid for the bridge configurations and ground motion records considered, and no general conclusions are the intention of this study. Further studies considering a wider range of bridge configurations (e.g., span length, piers height and corrosion ratios) are necessary for future research to investigate the effect of unbalanced seismic response of spatially variable corroded multi-span RC bridges. Nevertheless, the modelling methodology presented in this article provides some guidelines for practicing structural/bridge engineers to use in the seismic performance assessment of corrosion-damaged irregular concrete bridges. It is recommended to use the modelling technique in this article along with inspection data (e.g. non-destructive testing such as half-cell potential tests and corrosion rate tests) and construction drawings (for geometry and reinforcement details) to analyse and assess the time-dependent residual capacity of ageing irregular concrete bridges subject to various corrosion damage scenarios.

Disclosure statement

The authors report there are no competing interests to declare.

ORCID

Ebrahim Afsar Dizaj  <http://orcid.org/0000-0002-7755-9983>

Mohammad R. Salami  <http://orcid.org/0000-0003-0429-5398>
 Mohammad M. Kashani  <http://orcid.org/0000-0003-0008-0007>

References

- AASHTO. (2012). *AASHTO LRFD bridge design specifications*. Washington, DC: AASHTO.
- Afsar Dizaj, E. (2022). Modelling strategy impact on structural assessment of deteriorated concrete bridge columns. *Proceedings of the Institution of Civil Engineers - Bridge Engineering*, 175(4), 246–262. doi:10.1680/jbren.21.00003
- Afsar Dizaj, E., & Kashani, M. M. (2022a). Influence of ground motion type on nonlinear seismic behaviour and fragility of corrosion-damaged reinforced concrete bridge piers. *Bulletin of Earthquake Engineering*, 20(3), 1489–1518. doi:10.1007/s10518-021-01297-5
- Afsar Dizaj, E., & Kashani, M. M. (2022b). Nonlinear structural performance and seismic fragility of corroded reinforced concrete structures: modelling guidelines. *European Journal of Environmental and Civil Engineering*, 26(11), 5374–5403. doi:10.1080/19648189.2021.1896582
- Afsar Dizaj, E., & Kashani, M. M. (2020). Numerical investigation of the influence of cross-sectional shape and corrosion damage on failure mechanisms of RC bridge piers under earthquake loading. *Bulletin of Earthquake Engineering*, 18(10), 4939–4961. doi:10.1007/s10518-020-00883-3
- Afsar Dizaj, E., Salami, M. R., & Kashani, M. M. (2022a). Nonlinear dynamic behaviour and seismic fragility analysis of irregular multi-span RC bridges. *Structures*, 44, 1730–1750. doi:10.1016/j.istruc.2022.08.112
- Afsar Dizaj, E., Salami, M. R., & Kashani, M. M. (2022b). Seismic vulnerability assessment of ageing reinforced concrete structures under real mainshock-aftershock ground motions. *Structure and Infrastructure Engineering*, 18(12), 1674–1690. doi:10.1080/15732479.2021.1919148
- Akbari, R. (2010). Cyclic response of RC continuous span bridges with irregular configuration in longitudinal direction. *Structure and Infrastructure Engineering*, 9(2), 1–11. doi:10.1080/15732479.2010.510528
- Akbari, R. (2012). Seismic fragility analysis of reinforced concrete continuous span bridges with irregular configuration. *Structure and Infrastructure Engineering*, 8(9), 873–889. doi:10.1080/15732471003653017
- Akbari, R., & Maalek, S. (2018). A review on the seismic behaviour of irregular bridges. *Proceedings of the Institution of Civil Engineers - Structures and Buildings*, 171(7), 552–580. doi:10.1680/jstbu.17.00081
- American Society of Civil Engineers. (2021). Report card for America's infrastructure. <http://www.infrastructurereportcard.org>.
- Akiyama, M., Frangopol, D. M., & Matsuzaki, H. (2011). Life-cycle reliability of RC bridge piers under seismic and airborne chloride hazards. *Earthquake Engineering & Structural Dynamics*, 40(15), 1671–1687. doi:10.1002/eqe.1108
- California Department of Transportation. (2013). *Seismic Design Criteria Version 1.7*. Sacramento, CA: Engineering Service Center, Earthquake Engineering Branch.
- CEN 1998-2. (2005). *Eurocode 8: Design of structures for earthquake resistance, Part 2: Bridges*. Brussels, Belgium: European Committee for Standardization.
- Choe, D. E., Gardoni, P., Rosowsky, D., & Haukaas, T. (2009). Seismic fragility estimates for reinforced concrete bridges subject to corrosion. *Structural Safety*, 31(4), 275–283. doi:10.1016/j.strusafe.2008.10.001
- Cui, F., Zhang, H., Ghosn, M., & Xu, Y. (2018). Seismic fragility analysis of deteriorating RC bridge substructures subject to marine chloride-induced corrosion. *Engineering Structures*, 155, 61–72. doi:10.1016/j.engstruct.2017.10.067
- Dhakal, R. P., & Maekawa, K. (2002). Reinforcement stability and fracture of cover concrete in reinforced concrete members. *Journal of Structural Engineering*, 128(10), 1253–1262. doi:10.1061/(ASCE)0733-9445(2002)128:10(1253)

- Dizaj, E. A., Padgett, J. E., & Kashani, M. M. (2021). A Markov chain-based model for structural vulnerability assessment of corrosion-damaged reinforced concrete bridges. *Philosophical Transactions. Series A, Mathematical, Physical, and Engineering Sciences*, 379(2203), 20200290. doi:10.1098/rsta.2020.0290
- Dizaj, E. A., Madandoust, R., & Kashani, M. M. (2018a). Probabilistic seismic vulnerability analysis of corroded reinforced concrete frames including spatial variability of pitting corrosion. *Soil Dynamics and Earthquake Engineering*, 114, 97–112. doi:10.1016/j.soildyn.2018.07.013
- Dizaj, E. A., Madandoust, R., & Kashani, M. M. (2018b). Exploring the impact of chloride-induced corrosion on seismic damage limit states and residual capacity of reinforced concrete structures. *Structure and Infrastructure Engineering*, 14(6), 714–729. doi:10.1080/15732479.2017.1359631
- Domaneschi, M., Pellicchi, C., De Iuliis, E., Cimellaro, G. P., Morgese, M., Khalil, A. A., & Ansari, F. (2020). Collapse analysis of the Polcevera viaduct by the applied element method. *Engineering Structures*, 214, 110659. doi:10.1016/j.engstruct.2020.110659
- FEMA P695. (2009). Quantification of building seismic performance factors. *Federal Emergency Management Agency*, Washington, DC: Federal Emergency Management Agency (FEMA).
- Guirguis, J. E. B., & Mehanny, S. S. F. (2013). Evaluating code criteria for regular seismic behavior of continuous concrete box girder bridges with unequal height piers. *Journal of Bridge Engineering*, 18(6), 486–498. doi:10.1061/(ASCE)BE.1943-5592.0000383
- Ghosh, J., & Sood, P. (2016). Consideration of time-evolving capacity distributions and improved degradation models for seismic fragility assessment of aging highway bridges. *Reliability Engineering & System Safety*, 154, 197–218. doi:10.1016/j.res.2016.06.001
- Ge, X., Dietz, M. S., Alexander, N. A., & Kashani, M. M. (2020). Nonlinear dynamic behaviour of severely corroded reinforced concrete columns: Shaking table study. *Bulletin of Earthquake Engineering*, 18(4), 1417–1443. doi:10.1007/s10518-019-00749-3
- Hu, Y., & Guo, W. (2020). Seismic response of high-speed railway bridge-track system considering unequal-height pier configurations. *Soil Dynamics and Earthquake Engineering*, 137, 106250. doi:10.1016/j.soildyn.2020.106250
- Hwang, H., Liu, J. B., & Chiu, Y.-H. (2001). Seismic fragility analysis of highway bridges. <http://hdl.handle.net/2142/9267>.
- Ishac, M. G., & Mehanny, S. S. F. (2017). Do mixed pier-to-deck connections alleviate irregularity of seismic response of bridges with unequal height piers? *Bulletin of Earthquake Engineering*, 15(1), 97–121. doi:10.1007/s10518-016-9958-8
- Jara, J. M., Villanueva, D., Jara, M., & Olmos, B. A. (2013). Isolation parameters for improving the seismic performance of irregular bridges. *Bulletin of Earthquake Engineering*, 11(2), 663–686. doi:10.1007/s10518-012-9398-z
- Johnson, N., Ranf, R. T., Saiidi, M. S., Sanders, D., & Eberhard, M. (2008). Seismic testing of a two-span reinforced concrete bridge. *Journal of Bridge Engineering*, 13(2), 173–182. doi:10.1061/(ASCE)1084-0702(2008)13:2(173)
- Kappos, A. J., Manolis, G. D., & Moschonas, I. F. (2002). Seismic assessment and design of R/C bridges with irregular configuration, including SSI effects. *Engineering Structures*, 24(10), 1337–1348. doi:10.1016/S0141-0296(02)00068-8
- Karsan, I. D., & Jirsa, J. O. (1969). Behaviour of concrete under compressive loading. *Journal of the Structural Division*, 95(12), 2543–2564. doi:10.1061/JSDEAG.0002424
- Kashani, M. M., Lowes, L. N., Crewe, A. J., & Alexander, N. A. (2016). Nonlinear fibre element modelling of RC bridge piers considering inelastic buckling of reinforcement. *Engineering Structures*, 116, 163–177. doi:10.1016/j.engstruct.2016.02.051
- Kashani, M. M., Lowes, L. N., Crewe, A. J., & Alexander, N. A. (2015). Phenomenological hysteretic model for corroded reinforcing bars including inelastic buckling and low-cycle fatigue degradation. *Computers & Structures*, 156, 58–71. doi:10.1016/j.compstruc.2015.04.005
- Kashani, M. M., Crewe, A. J., & Alexander, N. A. (2013). Use of a 3D optical measurement technique for stochastic corrosion pattern analysis of reinforcing bars subjected to accelerated corrosion. *Corrosion Science*, 73, 208–221. doi:10.1016/j.corsci.2013.03.037
- Liu, X., Jiang, H., & He, L. (2017). Experimental investigation on seismic performance of corroded reinforced concrete moment-resisting frames. *Engineering Structures*, 153, 639–652. doi:10.1016/j.engstruct.2017.10.034
- Mander, J. B., Priestley, M. J. N., & Park, R. (1988). Observed stress-strain behavior of confined concrete. *Journal of Structural Engineering*, 114(8), 1827–1849. doi:10.1061/(ASCE)0733-9445(1988)114:8(1827)
- Meda, A., Mostosi, S., Rinaldi, Z., & Riva, P. (2014). Experimental evaluation of the corrosion influence on the cyclic behaviour of RC columns. *Engineering Structures*, 76, 112–123. doi:10.1016/j.engstruct.2014.06.043
- McKenna, F. (2011). OpenSees: A framework for earthquake engineering simulation. *Computing in Science & Engineering*, 13(4), 58–66. doi:10.1109/MCSE.2011.66
- Mergos, P. E., & Kappos, A. J. (2013). A combined local damage index for seismic assessment of existing RC structures. *Earthquake Engineering & Structural Dynamics*, 42(6), 833–852. doi:10.1002/eqe.2247
- Mitoulis, S. A., & Rodriguez, J. R. (2017). Seismic performance of novel resilient hinges for columns and application on irregular bridges. *Journal of Bridge Engineering*, 22(2), 4016114. doi:10.1061/(ASCE)BE.1943-5592.0000980
- Priestley, M. J. N. (2007). The need for displacement-based design and analysis. *Advanced earthquake engineering analysis*, vol. 494, Vienna, Austria: CISM International Center for Mechanical Sciences, Springer, 121–132
- Ramanathan, K. N. (2012). Next generation seismic fragility curves for California bridges incorporating the evolution in seismic design philosophy [PhD thesis]. Georgia Institute of Technology.
- Sajed, M., & Tehrani, P. (2020). Effects of column and superstructure irregularity on the seismic response of four-span RC bridges. *Structures*, 28, 1400–1412. doi:10.1016/j.istruc.2020.09.057
- Salami, M. R., Afsar Dizaj, E., & Kashani, M. M. (2021). Fragility analysis of rectangular and circular reinforced concrete columns under bidirectional multiple excitations. *Engineering Structures*, 233, 111887. doi:10.1016/j.engstruct.2021.111887
- Schmitt, G. (2009). *Global needs for knowledge dissemination, research, and development in materials deterioration and corrosion control*. New York: World Corrosion Organization.
- Soltanieh, S., Memarpour, M. M., & Kilanehi, F. (2019). Performance assessment of bridge-soil-foundation system with irregular configuration considering ground motion directionality effects. *Soil Dynamics and Earthquake Engineering*, 118, 19–34. doi:10.1016/j.soildyn.2018.11.006
- Vu, K. A. T., & Stewart, M. G. (2000). Structural reliability of concrete bridges including improved chloride-induced corrosion models. *Structural Safety*, 22(4), 313–333. doi:10.1016/S0167-4730(00)00018-7
- Xiang, N., & Li, J. (2020). Utilizing yielding steel dampers to mitigate transverse seismic irregularity of a multispan continuous bridge with unequal height piers. *Engineering Structures*, 205, 110056. doi:10.1016/j.engstruct.2019.110056
- Zhang, M., Akiyama, M., Shintani, M., Xin, J., & Frangopol, D. M. (2021). Probabilistic estimation of flexural loading capacity of existing RC structures based on observational corrosion-induced crack width distribution using machine learning. *Structural Safety*, 91, 102098. doi:10.1016/j.strusafe.2021.102098
- Zhang, Y., DesRoches, R., & Tien, I. (2019). Impact of corrosion on risk assessment of shear-critical and short lap-spliced bridges. *Engineering Structures*, 189, 260–271. doi:10.1016/j.engstruct.2019.03.050